Petroleum Science 18 (2021) 1840–1859

Contents lists available at ScienceDirect

Petroleum Science

journal homepage: www.keaipublishing.com/en/journals/petroleum-science

Original Paper

Research on *in-situ* condition preserved coring and testing systems

He-Ping Xie [a, b, c], Tao Liu [e, *], Ming-Zhong Gao [a, b, c], Ling Chen [d], Hong-Wei Zhou [f], Yang Ju [f, g], Feng Gao [g], Xiao-Bo Peng [a, b], Xiong-Jun Li [a, b], Rui-Dong Peng [f], Ya-Nan Gao [g], Cong Li [a, b, c], Zhi-Qiang He [a, b, c], Ming-Qing Yang [a, b, c], Zhi-Yu Zhao [a, b, e]

[a] *Guangdong Provincial Key Laboratory of Deep Earth Sciences and Geothermal Energy Exploitation and Utilization, Institute of Deep Earth Sciences and Green Energy, College of Civil and Transportation Engineering, Shenzhen University, Shenzhen, 518060, Guangdong, China*
[b] *Shenzhen Key Laboratory of Deep Underground Engineering Sciences and Green Energy, Shenzhen University, Shenzhen, 518060, Guangdong, China*
[c] *MOE Key Laboratory of Deep Earth Science and Engineering, College of Water Resource and Hydropower, Sichuan University, Chengdu 610065, Sichuan, China*
[d] *School of Mechanical Engineering, Sichuan University, Chengdu, 610065, Sichuan, China*
[e] *Institute of New Energy and Low-Carbon Technology, Sichuan University, Chengdu, 610065, Sichuan, China*
[f] *State Key Laboratory of Coal Resources and Safe Mining, China University of Mining and Technology (Beijing), Beijing, 100083, China*
[g] *Frontier Science Research Center for Fluidized Mining of Deep Underground Resources, China University of Mining and Technology, Xuzhou, 221116, Jiangsu, China*

ARTICLE INFO

Article history:
Received 12 July 2021
Accepted 28 October 2021
Available online 10 November 2021

Edited by Yan-Hua Sun

Keywords:
Deep mining
In-situ environmental conditions
In-situ condition preserved coring and testing
In-situ transfer
Deep-earth processes
ICP-Coring
In-situ condition-preserved coring

ABSTRACT

As shallow resources are increasingly depleted, the mechanics' theory and testing technology of deep *in-situ* rock has become urgent. Traditional coring technologies obtain rock samples without retaining the *in-situ* environmental conditions, leading to distortion of the measured parameters. Herein, a coring and testing systems retaining *in-situ* geological conditions is presented: the coring system that obtains *in-situ* rock samples, and the transfer and testing system that stores and analyzes the rocks under a reconstructed environment. The ICP-Coring system mainly consists of the pressure controller, active insulated core reactor and insulation layer and sealing film. The ultimate bearing strength of 100 MPa for pressure-preservation, temperature control accuracy of 0.97% for temperature-retained are realized. CH_4 and CO permeability of the optimized sealing film are as low as 3.85 and 0.33 ppm/min. The average tensile elongation of the film is 152.4% and the light transmittance is reduced to 0%. Additionally, the pressure and steady-state temperature accuracy for reconstructing the *in-situ* environment of transfer and storage system up to 1% and ±0.2 is achieved. The error recorded of the noncontact sensor ring made of low-density polymer is less than 6% than that of the contact test. The system can provide technical support for the deep *in-situ* rock mechanics research, improving deep resource acquisition capabilities and further clarifying deep-earth processes.

1. Introduction

With the gradual depletion of shallow resources, the mining of deep resources is becoming common (Gao et al., 2018a; Pang et al., 2015; Xie et al., 2015, 2019; Zhang et al., 2016). At present, the exploitation of deep resources is an engineering priority that requires technological integration and theoretical development. There is a lack of transformative technology suitable for deep engineering. Deep rock exhibits nonlinear mechanical behavior in an *in-situ* environment (Gao et al., 2021a). The applicability of the existing fundamental theories and engineering technologies of rock mass mechanics needs to be further studied. The basic physical and mechanical properties (density, porosity, Poisson's ratio, elastic modulus, etc.) obtained based on standard core samples do not reflect the effects of *in-situ* environmental conditions (such as temperature and pressure). Such properties may exhibit a linear or nonlinear behavior in an *in-situ* environment (Gao et al., 2020a,b,c; Guo et al., 2020; Man and Zhou, 2010; Zhang et al., 2019b; Zhou et al., 2010; Zuo et al., 2011). In addition, in the present research methods, the physical and mechanical properties of rocks are tested

* Corresponding author.
E-mail address: liutao3200023@scu.edu.cn (T. Liu).

https://doi.org/10.1016/j.petsci.2021.11.003

Abbreviations

APCs	Advanced piston corers
AIST	National Institute of Advanced Industrial Science and Technology
BIO	Bicrobial reaction chamber
CDC	Controlled depressurization chamber
CNPC	China National Petroleum Corporation
DAPC	Dynamic autoclave piston corer
DSC	Direct shear chamber
DSDP	Deep-sea drilling project
ESC	Effective stress chamber
FPC	Fugro pressure corer
GHOBS	Gas Hydrate Ocean Bottom Simulator
HRC	HYACE Rotary Corer
HYACE	Hydrate coring equipment system
ILP-Coring	*In-situ* light-preserved coring
IMP-Coring	*In-situ* moisture-preserved coring
IPP-Coring	*In-situ* pressure-preserved coring
ISP-Coring	*In-situ* substance-preserved coring
ITP-Coring	*In-situ* temperature-preserved coring
JOGMEC	Japan Oil, Gas and Metals National Corporation
KIGAM	Korea Institute of Geoscience and Mineral Resources
MAC	Multiple autoclave corer
ODP	Ocean Drilling Program
PCBs	Pressure core barrels
PCSs	Pressure core samplers
PTCS	Pressure temperature core sampler
IPTC	Instrumented Pressure Testing Chamber
PCCTs	Pressure Core Characterization Tools
PNATs	Pressure-core Nondestructive Analysis Tools
JAMSTEC	Japan Marine Science and Technology Agency
PTPS	Pressure and temperature preservation system
TACTT	Transparent acrylic cell triaxial testing system

using a standard core and a classical load path based on the classical theories of rock mechanics and the experimental methods of elastic-plastic mechanics.

The physical and mechanical properties of rock materials are disturbed during coring. Furthermore, standard core analysis does not consider the deep *in-situ* conditions and the disturbance of deep engineering (Yang and Guo, 2020). Thus, the obtained properties, models, and theories ignore engineering disturbances (Gao et al., 2018b, Gao et al., 2021b). Thus, the deep resource development is hindered, making it difficult to achieve the safe, efficient, and economic exploitation.

Therefore, developing theoretical and technological systems of rock mechanics that take into account the deep *in-situ* environment becomes essential. The challenges are how to achieve deep *in-situ* condition-preserved coring (ICP-Coring), testing, and analysis. Nevertheless, there is still a lack of deep *in-situ* rock mechanics research worldwide due to a lack of technology appropriate for the *in-situ* investigation of rock properties. The priority is to obtain rock samples that preserve the *in-situ* environment (pressure, temperature, etc.). Conventional coring technologies have significant limitations, among which pressure-retaining coring technology mainly focuses on oil and gas exploration, geological and mineral exploration, and marine combustible ice sampling operations (Khizar et al., 2015; Dickens et al., 2000; Kvenvolden et al., 1983; Milkov et al., 2004; Priest et al., 2015) and considers only the retention of *in-situ* pressure.

Furthermore, the current maximum bearing capacity of the pressure coring sampler is 70 MPa (Rothwell and Rack, 2006), far from meeting the needs of deep exploration. Thermal insulation coring technology focuses predominantly on minimizing core temperature drops and cannot achieve active thermal insulation. In recent years, many international organizations have developed coring tools with thermal insulation and pressure retention functions (Li et al., 2006; Zhang et al., 2006; Zhu et al., 2013), such as the Japan National Oil Corporation and China First Institute of Oceanography. The technology is still in the experimental stage and not yet ready for widespread application. Freezing sampling technology (Sun et al., 2015; Wei et al., 2020) is effective in the acquisition of natural gas hydrate. However, it changes the occurrence temperature and pressure and destroys the original mechanical characteristics of the samples. Protective fluid coring technology can cover the core sample in a protective fluid (Su, 2019) to prevent it from being contaminated by drilling fluids without integrating pressure- and temperature-preserving functions. Clearly, conventional coring technologies are generally designed to preserve only one *in-situ* environmental property. Obtaining critical information such as the *in-situ* pore pressure, temperature, humidity, and microbial environment simultaneously with core samples is impossible with existing technologies, which significantly limits the research significance of deep cores. This paper proposes a coring and testing system retaining the *in-situ* geological conditions of deep rocks to enhance the accuracy of deep exploration.

The technological challenges of *in-situ* testing of deep rocks need to be addressed. The cores acquired through traditional testing technology are directly exposed, meaning that the state of the cores cannot be held constant in sample preparation processes. It is impossible to measure physical and mechanical properties in the *in-situ* states. Moreover, *in-situ* testing technology is developed mainly in the field of noncontact testing (wave techniques, electromagnetic techniques, X-ray diffraction, etc.) (Priest et al., 2015). There are two main types of noncontact testing: Firstly, taking core samples using the conventional coring system and testing the temperature and pressure of the core with built-in sensors without opening the core barrel (Hohnberg et al., 2003; Qin et al., 2005). Secondly, testing with reconstructing the original environment of occurrence (Lee et al., 2013; Schultheiss et al., 2011). None of these technologies have integrated true triaxial compressive testing methods (Priest et al., 2015). There are significant limitations in environmental reconstruction. The most advanced testing technology is capable of reconstructing a testing environment with a pressure up to 35 MPa and a temperature up to 50 °C (Schultheiss et al., 2017), which completely fails to meet the needs of the testing and analysis of the physical and mechanical behavior, chemical composition, and organic resources of deep rock (Xie et al., 2020b). Consequently, deep *in-situ* mechanical physical, chemical, and microbiological characteristics cannot be obtained (Kashefi and Lovley, 2003). Many defects among the existing testing technologies remain, such as a limited capacity to reconstruct *in-situ* environmental pressure and temperature, an inability to perform high-precision preparation of samples in a reconstructed environment, and a lack of integration of the triaxial testing function (Priest et al., 2015; Schultheiss et al., 2017). There is a theoretical and technological gap in the reconstruction of the *in-situ* environment of deep rock formations and thus the preparation, transfer and testing of standard cores.

In general, there is a need for deep *in-situ* rock mechanics theory and technology that are suitable for use in deep resource

exploitation. The critical issue lies in ascertaining the physical and mechanical behavior of rocks at different depths and revealing the fundamental differences between deep and shallow structures. This paper proposes a coring and testing system that can retain *in-situ* geological conditions. Functional designs for ICP-Coring, environmental reconstruction, sample transfer, preparation, triaxial loading tests, etc. are proposed. Additionally, this innovation work is supported by "*In-situ* coring and fidelity testing analysis system for deep rock", a major scientific research instrument program of National Natural Science Foundation of China.

The established system is expected to address current technological deficiencies and ensure that cores remain in the *in-situ* state during the entire process from deep ICP-Coring, ground transfer and storage, sample preparation, and mechanical testing. The study provides support for establishing new theories of deep engineering and enhances deep resource acquisition capabilities.

2. The current situation of *in-situ* coring and testing technologies

2.1. Conventional coring technology related to gas-hydrate-bearing sediment sampling

In seabed sediment, natural gas hydrates (combustible ice) are formed under conditions within a specific temperature and pressure range (Wang et al., 2021). When a core with natural gas hydrates is lifted to the sea surface at ambient temperature and pressure, all or most of the material components of the natural gas hydrates will decompose (Kim et al., 2021; Skiba et al., 2020). It is imperative to account for the physical properties of natural gas hydrates during coring, which has led international scientific research institutions to explore pressure- and temperature-preserving coring techniques (Rothwell and Rack, 2006; Wang et al., 2020).

In-situ temperature-preserved coring (ITP-Coring) and *in-situ* pressure-preserved coring (IPP-Coring) technology can hold the obtained core at its *in-situ* pressure and temperature conditions throughout the operational process. In contrast, conventional coring tools are not equipped with temperature and pressure preserving devices, making it difficult to obtain rock cores under their natural temperature and pressure conditions. At present, representative deep-sea coring devices include the Pressure Core Barrel (PCB) deployed by the International Deep-Sea Drilling Project (DSDP) (Dickens et al., 2000; Kvenvolden et al., 1983) and the Advanced Piston Corer (APC) and Pressure Core Sampler (PCS) (Milkov et al., 2004) deployed in the International Ocean Drilling Project and Ocean Drilling Program. The Hydrate Autoclave Coring Equipment (HY-ACE) adopts the Fugro Pressure Corer (FPC) and the HY-ACE Rotary Corer (HRC) (Amann et al., 2021; Schultheiss et al., 2009); Japan developed a Pressure-Temperature Core Sampler (PTCS) (Wakishima et al., 1998); deep-ocean researchers deployed the Multiple Autoclave Corer (MAC) and dynamic high-pressure Dynamic Autoclave Piston Corer (DAPC) from the R.V.SONNE (Bohrmann et al., 2007; Heeschen et al., 2007; Hohnberg et al., 2003); Zhejiang University developed a gravity piston-type natural gas hydrate corer (Chen et al., 2006; Qin et al., 2005); the First Institute of Oceanography in China developed a deep-water and shallow-hole natural gas hydrate coring drill with temperature and pressure preserving functions (Zhang et al., 2006); Zhu et al. (2013) developed a Pressure and Temperature Preservation System (PTPS) for natural gas hydrate coring; Qin et al. developed a handheld mechanical sedimentary coring device (Qin et al., 2005). In addition, some scholars have conducted systematic research into deep sea hydrothermal *in-situ* sampling technology (Wu, 2008) and Antarctic glacier *in-situ* coring technology (Hodgson et al., 2016). In the field of deep-sea exploration, the existing conventional coring tools can preliminarily achieve partial pressure or compensating functions. The bearing capacity of PCS is 70 MPa, that of PCB and PTCS is 30 MPa, that of FPC and HRC is 25 MPa, and that of MAC and DAPC is 20 MPa. Pressure is preserved through a mechanical valve called a pressure controller, such as a rotary ball valve. The existing IPP-Coring technology essentially relies on the hydrostatic pressure of seawater, and the corresponding pressure retention capacity depends on the occurrence environment where the cores are taken.

The establishment of ICP-Coring systems is a challenging endeavor. Presently, only PTCS and PTPS provide partial ITP-Coring. The PTCS maintains temperature through an adiabatic and thermoelectric tube. The pressure is maintained with a ball valve, and the temperature is maintained with a battery-powered thermoelectric cooling device. This device preserves temperature by adding thermal insulation materials, charging the sample with liquid nitrogen, and utilizing a drilling fluid cooling device. The PTPS adopts a double-layer passive temperature preservation system that is maintained by spraying an insulation layer onto the inner surface and covering the outer surface with an anti-ultraviolet coating, combined with an interlayer vacuum. The insulation layer and double-layer vacuum structure minimize heat exchange (Dell'Agli and Mascolo, 2000; Di Girolamo et al., 2010). Coring systems are barely capable of active temperature preservation. They adopt the core-freezing method, where the rock core is placed in a specially designed device as soon as the core barrel reaches the ground. The core temperature is preserved by performing measures such as rapid ice covering or liquid nitrogen freezing. Evidently, achieving temperature preservation with the existing technologies is challenging, as they essentially focus on temperature control and compensation. In addition, ICP-Coring is different from seabed sediment coring, and continental rock cores tend to be collected from high-temperature environments. During coring, ITP-Coring technology prevents the temperature of the core from dropping during recovery, while the temperature of the core is prevented from increasing when recovering coring seabed sediment. Hence, the existing ITP-Coring are not directly applicable to that of deep rock formations. Further investigations of technologies better suited for such purposes are necessary.

In conclusion, the current coring technology of seabed sediment is actually limited to the conventional "hermetic coring" concept, which retains *in-situ* pressure rather than delivering true *in-situ* coring. The present coring technologies are largely concentrated in areas that require pressure retention, temperature preservation, and pollution prevention. Temperature-preservation technologies are predominantly passive, as active temperature preservation poses greater challenges. However, some microorganisms are extremely dependent on the *in-situ* occurrence environment. In the absence of suitable coring technology, living organisms (microorganisms, viruses, etc.) entrapped in deep rock samples may die. There is an urgent need to develop ICP-Coring technology for deep rock formations to cultivate living organisms (microbes, viruses, etc.) in deep rocks and facilitate future scientific exploration.

2.2. Conventional continental coring principles and technologies

Globally, scientific drilling (continental coring) has become an indispensable, essential means for addressing major problems on topics such as deep resources, disasters, and the environment. Since the 1950s, drilling projects, including the US Mohole Drilling Project (MDP), the German Continental Deep Drilling Program (Kontinentales Tiefbohr Programm, KTB), the Iceland Deep Drilling Project, the International Continental Scientific Drilling Program

(ICDP), and the China Songke Scientific Drilling Program, have attracted worldwide attention (Coney et al., 2007; Dickens et al., 2003; Friðleifsson et al., 2010, 2011, 2017; Fulthorpe et al., 2008; Litt et al., 2009; Osborne et al., 2011; Yetginer and Tjelta, 2010; Yun, 2005). The critical task of all scientific drilling projects is to explore the structure and evolution of deep strata, paleoclimates, and paleoenvironments.

ITP-Coring is crucial for the evaluation of oil saturation and natural gas reserves. For continental pressure-retaining coring, the China National Petroleum Corporation (CNPC) Greatwall Drilling Company has developed the GW-CP194-80A IPP-Coring tool capable of pressure-retaining coring operations with a diameter of 80 mm and a length of 6 m. The pressure-retention capacity can reach up to 60 MPa (Yang et al., 2020) by triggering the ball valve seal via differential assembly. The Xi'an Research Institute of China Coal Science and Industry Group has developed a hermetic coring device for accurately measuring the coal seam methane content in underground and surface coal mines. The tool system is capable of extracting cores with a diameter of 38 mm and a length of 1.2 m by relying on a ball valve seal for hermetic pressure preservation. Nevertheless, its maximum pressure-preserving capacity is only 10 MPa, which meets the technical requirements of only coal seam methane determination (Sun et al., 2020). The American Halliburton Company has developed wireline rotary sidewall coring equipment; however, the cores taken via this system are small in diameter and short in length; the cores are extracted in multiple sections, and all core sections are stored in the same sealed cavity without retaining the *in-situ* pressure of the cores (Pinkett and Westacott, 2016).

Conventional coring technologies focus on the efficiency and depth of core acquisition (Wang et al., 2014). Although there has been some research on ITP-Coring and IPP-Coring technology, *in-situ* substance-preserved coring (ISP-Coring), *in-situ* moisture-preserved coring (IMP-Coring) and *in-situ* light-preserved coring (ILP-Coring) are still unavailable due to a technological failure to effectively seal oil and gas and other resources inside the core, leading to partial or complete loss of the pressure, temperature, pore water, chemical and biological information of the *in-situ* environment of the core; only “ordinary cores” can be obtained. Severe distortion of such cores will result in the failure to measure the physical and mechanical properties in the actual conditions of deep rock formations due to stress release, the distortion of the evaluation of oil and gas resources, and the death of living organisms entrapped in the deep rock formations. Thus, the mechanics, physics, chemistry, microbiology, and other characteristics of deep rocks obtained with traditional drilling and coring technology are not accurate. To enhance the accuracy and scientific exploration of deep-earth scientific laws, it is imperative to develop proper ICP-Coring technology for acquiring “living” samples of rock masses to facilitate in-depth research into the scientific laws of deep geoscience.

2.3. Deep in-situ transfer and testing technology

Deep *in-situ* transfer and testing technology seeks to measure core properties and establish theories under *in-situ* environmental conditions. To preserve the pressure, physical, chemical, and biological conditions of the cores, the challenging problem involving transferring cores in the *in-situ* state needs to be resolved, i.e., the technology required for connecting the coring system with the testing system needs to be developed.

Currently, the available *in-situ* core testing technology performs only noncontact measurement, primarily for the noncontact testing (via waves and electromagnetics) of seabed sedimentary cores, and lacks the capability to perform mechanical testing with real-time loading. As a result, the scientific value of cores cannot be maximized. GOM JIP Leg1 adopted the first high-pressure core testing device, the Instrumented Pressure Testing Chamber (IPTC) (Yun et al., 2006). In 2007, the Georgia Institute of Technology developed an effective stress chamber (ESC) to test the properties of hydrate-bearing sediments under *in-situ* temperature, pressure, and effective stress recovery conditions. This ESC has been further developed into the Gas Hydrate Ocean Bottom Simulator (GHOBS) of the Korea Institute of Geoscience and Mineral Resources (KIGAM) (Lee et al., 2009). Later, Georgia Tech developed a series of pressure core testing tools named the Pressure Core Characterization Tools (PCCTs) (Santamarina et al., 2012a, 2012b). PCCTs consist of a manipulator for core transferring, two sets of cutting devices, an ESC, a direct shear chamber (DSC), a controlled depressurization chamber (CDC), and a microbial reaction chamber (BIO) (Santamarina et al., 2015). In 2012, the National Institute of Advanced Industrial Science and Technology (AIST) developed the Pressure-core Nondestructive Analysis Tools (PNATs), which include a transparent acrylic cell triaxial testing system (TACTT) and X-radiography system (Jin et al., 2014; Nagao et al., 2015; Yoneda et al., 2015b). GeoTek's PCATS (Schultheiss et al., 2006; Suzuki et al., 2015) is capable of multiparameter scanning by noncontact means such as P-wave testing; during the testing process, the rock samples are covered and transferred to the scanning chamber while maintaining the pressure. Japan Marine Science and Technology Agency (JAMSTEC) and Associates Inc. both adopted PTCS technology (Qin et al., 2009; Schultheiss et al., 2011), which matches well with the PCATS to perform noncontact measurements of the pressure and temperature of the rock samples. In China, the gravity piston natural gas hydrate corer and the deep-water and shallow-hole temperature and pressure-retaining natural gas hydrate coring drill designed by Zhejiang University are capable of determining the pressure and temperature of rock samples without opening the core barrel (Yoneda et al., 2015a).

Nevertheless, none of the conventional testing technologies mentioned above can achieve the preparation, transfer, and mechanical testing of standard cores under *in-situ* conditions. There is a pressing need for further research and investigation on testing technology.

3. Research on the coring and testing systems retaining *in-situ* geological conditions

3.1. Research on deep ICP-Coring systems

3.1.1. IPP-Coring

IPP-coring technologies aim to keep the cores extracted at the *in-situ* pore pressure, providing indispensable information for resource exploration and geological engineering evaluation. Conventional coring tools cannot maintain the pressure, leading to irreversible changes in the physical properties and mechanical properties of core samples. Future exploration operations of deep resources may face extreme pressure of more than 10000 psi (approximately 69 MPa) (Ashena and Thonhauser, 2018), which is a significant challenge for deep IPP-Coring technology. There is an urgent need to carry out theoretical and technical research on deep IPP-Coring. The key to advancement lies in the optimized design of the pressure controllers of the coring device (He et al., 2019; Li et al., 2021).

The pressure controller is located at the lowest end of the core barrel to automatically seal the pressure chamber after the core is

Fig. 1. Schematic diagram of a pressure-preserved controller.

extracted. The pressure chamber determines the ultimate bearing strength of the pressure corer. The valve cover of the pressure controller is initially located between the inner and outer tubes of the corer (as shown in Fig. 1). When the core sample is cut, the inner tube is released from its locking position. Then, the valve cover is set in the valve seat. The main advantages of this setup are self-tightening sealing and a larger core diameter. Based on the pressure coring technology, the configuration and sealing capacity of the pressure maintaining controller was optimized. Based on the Steinmetz solid principle (Zhang et al., 2019a), this paper proposes five pressure controller configurations, of which A1, A2, and A3 are cone-shaped pressure controllers, type D is a spherical-cylindrical shell pressure controller, and type E is a saddle-shaped pressure controller. The structures of the pressure controllers are shown in Fig. 2.

To analyze the stress distribution and structural deformation of pressure controllers, the elastoplastic model of the ABAQUS numerical simulation software was used with the measured stress-strain data (304 stainless steel, yield strength 604.6 MPa). The boundary condition of the valve seat is fully constrained at the bottom, and a pressure load is gradually applied to the upper face of the valve cover. As the load increases, the edge of the minor axis of the valve cover produces a more significant displacement along the contact surface. The contact pressure at the potential leakage region decreases, as shown in Fig. 3. Therefore, the ultimate bearing strength of the pressure controller can be evaluated based on the fluctuation in the contact pressure. Numerical simulation results show that the maximum bearing strength of A1 is 27.8 MPa, that of A2 is 66.3 MPa, and that of A3 is 100.5 MPa. Under a water pressure of 200 MPa, the contact pressure of controllers D and E do not show a decreasing tendency. The equivalent stress contour plots of the pressure controllers under the ultimate load condition are shown in Fig. 4. Among them, the two wings of the conical pressure controller (A1/A2/A3) have a larger stress concentration, and the stresses of the spherical shell (D) and saddle (E) shapes are concentrated in the middle of the device. As the load increases, the major axis of the valve cover becomes the main support structure, while the minor axis of the valve cover retracts inward on both sides.

For directional drilling, the pressure controller needs to work in an oblique or horizontal angle. To make the pressure controller more extensive, the magnetic trigger pressure-preserved controller was proposed for the first time, as shown in Fig. 5. Magnetically triggered pressure controller uses the magnetic potential energy of the permanent magnet to generate trigger kinetic energy. When the valve cover is closed, the attraction between the permanent magnet and the magnetic material is used to make the valve cover tightly attracted. And this attraction can be used as the initial sealing force of pressure-preserved controllers. The magnetic trigger pressure-preserved controller completely overcomes the gravity on which the existing trigger depends. The magnetic triggering allows the pressure controller to achieve self-triggering closure by overcoming gravity when taking the center at any angles. Through numerical simulation, the magnetic triggering force can reach 150.74 N and the initial sealing force can reach 46.23 N. This fully validates the feasibility of the magnetically triggered pressure controller.

3.1.2. ITP-Coring

ITP-Coring is a global challenge. Internationally, temperature preservation has been limited to combustible ice coring, and the techniques used for maintaining temperature are passive, not active. The existing ITP-Coring technology used for subsea sediments cannot directly applicable because the cores of deep rock formations on land are often in a high-temperature environment. The purpose of ITP-Coring technology is to prevent the core temperature from dropping, while that of the existing ITP-Coring technology used for combustible ice is precisely the opposite.

In 2020, the idea of combining active and passive temperature preservation (Fig. 6) was put forward (He et al., 2020). Working

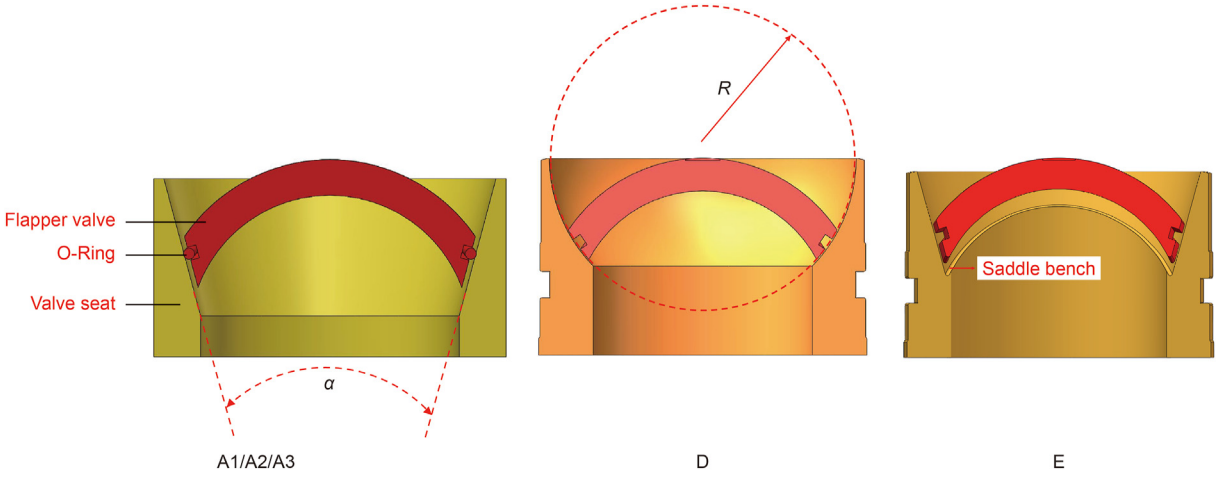

Fig. 2. 3D models of pressure controllers.

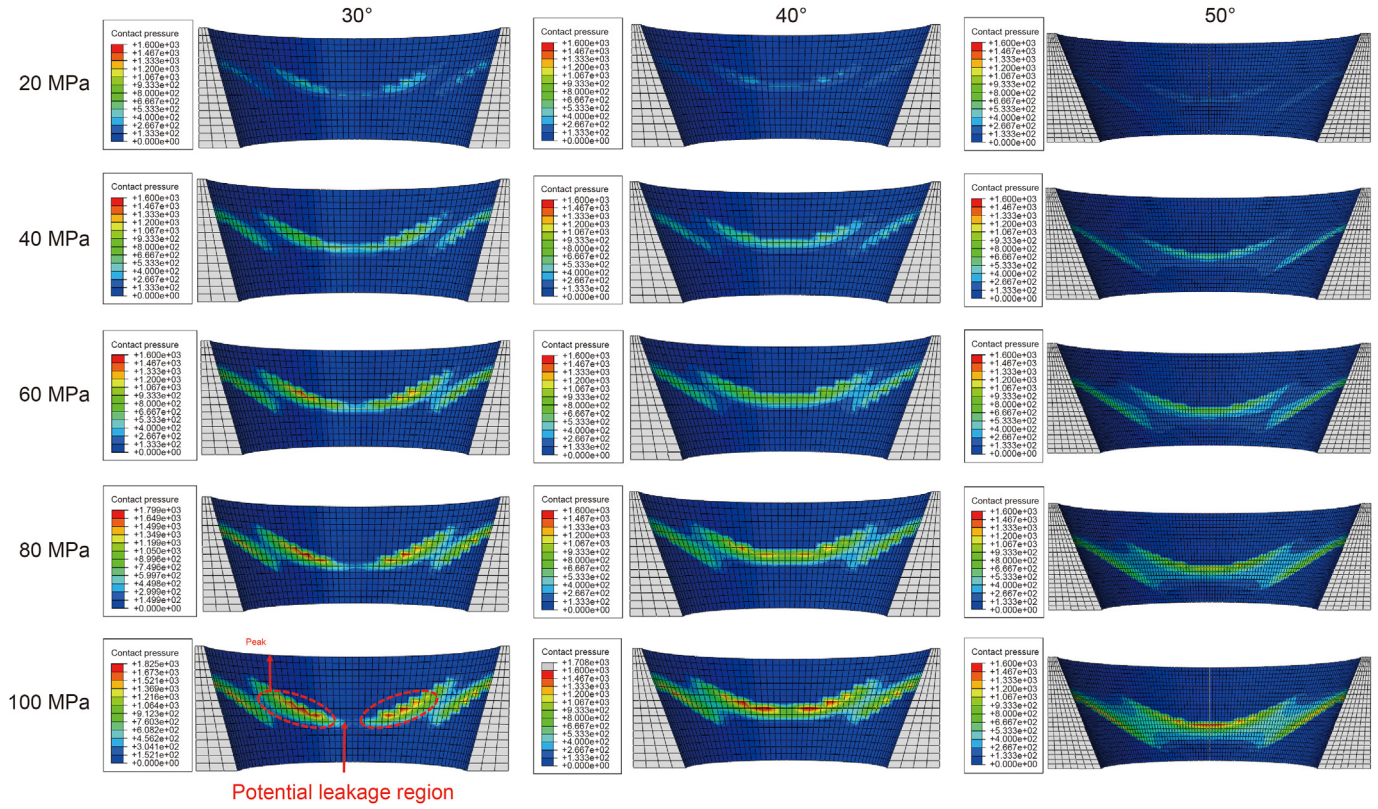

Fig. 3. The contact pressures for different angles of the conical contact surfaces.

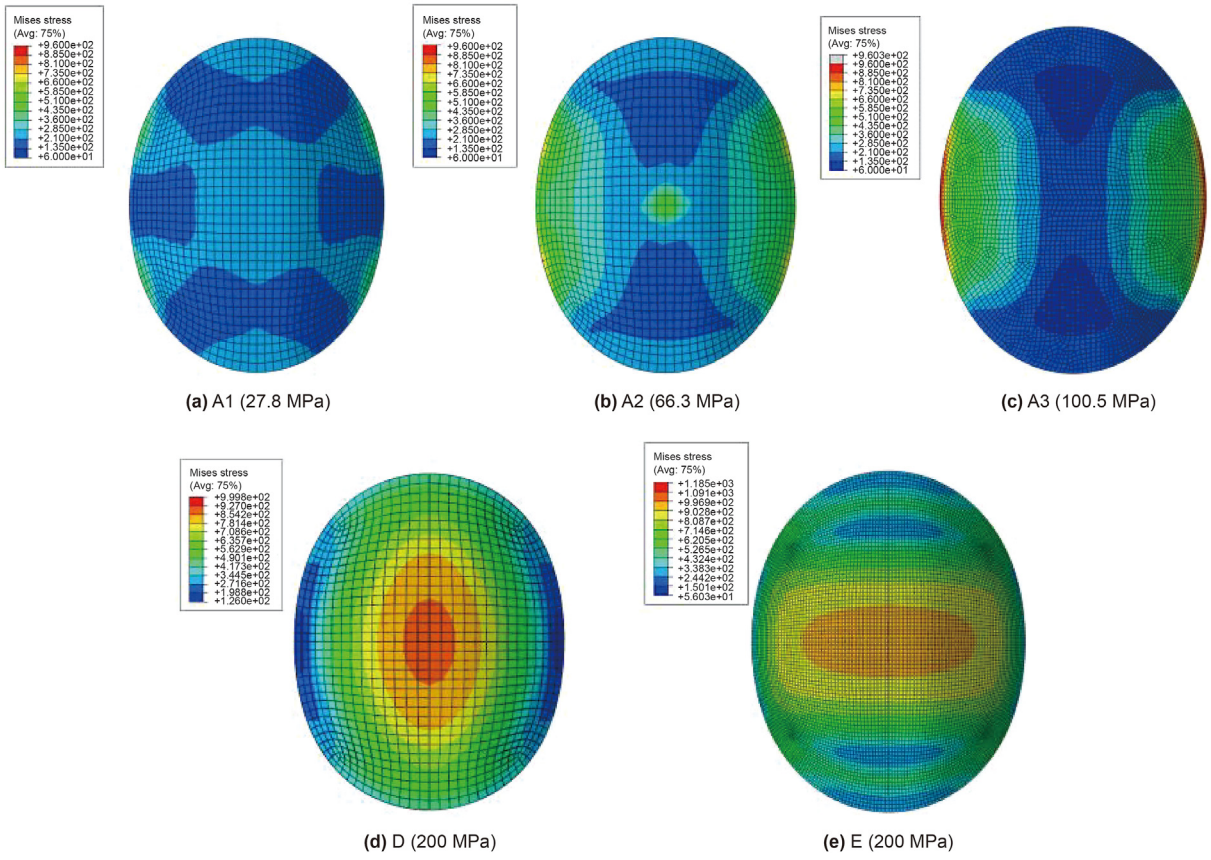

Fig. 4. Contour plots of the equivalent stresses of the critical loads of the pressure controllers.

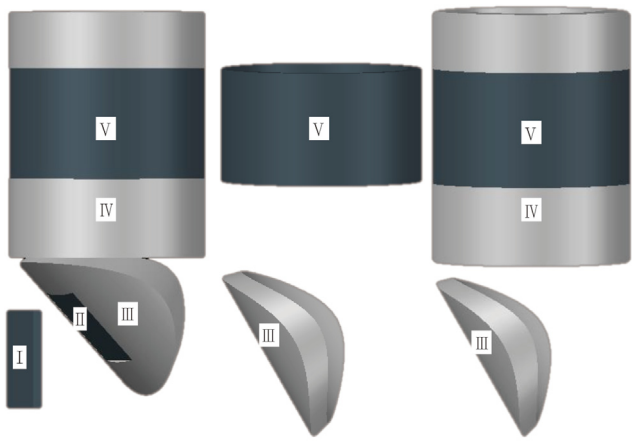

Fig. 5. Three schemes of magnetically triggered pressure controllers.

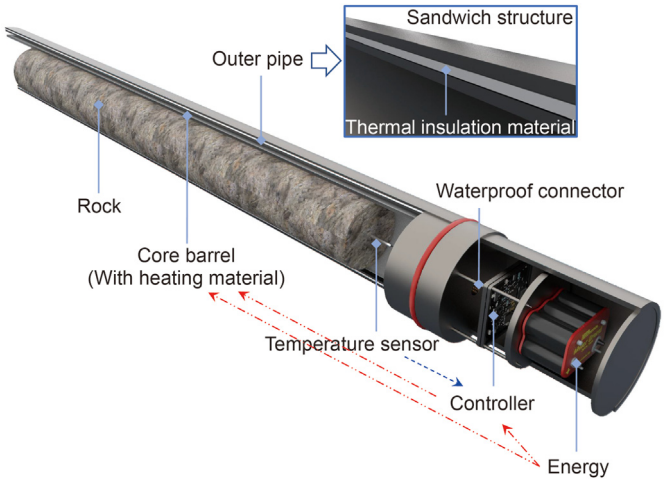

Fig. 6. Schematic diagram of the temperature-preservation structure of coring devices (He et al., 2020).

toward a breakthrough in the ITP-Coring technology of deep rocks, an initial investigation of core temperature variations and heat dissipation during core lifting has been conducted. A temperature-preservation testing system was established, and temperature control capability tests on active temperature-preservation technology was performed. Then, a passive temperature-preservation structure was proposed, and the passive insulation materials were optimized.

Studies have been conducted on the temperature variation and energy consumption of active temperature preservation during the core lifting process based on the theory of unsteady heat conduction (Yang and Tao, 2006), and the trend of the variation in temperature in the chamber during the actual core lifting process was obtained, as shown in Eq. (1).

$$T(t) = \frac{v\Delta T}{100}\left[c_w m_w R\left(1 - e^{-\frac{t}{c_w m_w R}}\right) - t\right] + 150 \quad (1)$$

where $T(t)$ is the temperature of the liquid at any time, °C; v is the lifting velocity of the coring device, m/s; ΔT is the ground temperature gradient of formations, °C/100 m; m_w and c_w are the mass (kg) and specific heat capacity (J/(kg·°C)) of the liquid in the

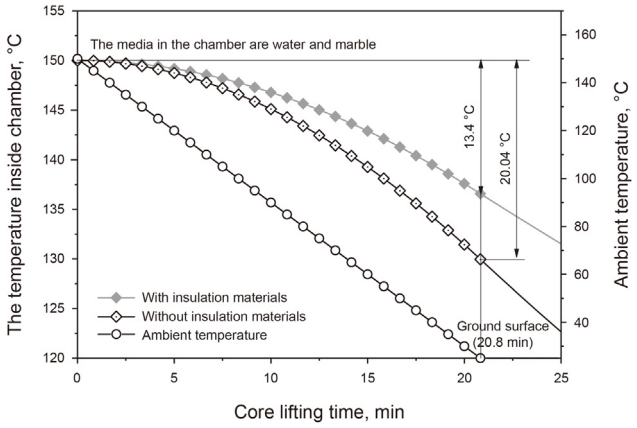

Fig. 7. Trends of the temperature variations in the core chamber during the coring process.

chamber, respectively; R is the total thermal resistance, °C/W; t represents time, s.

Taking the core lifting velocity of 2.5 m/s as an example, according to Eq. (1), when the geothermal gradient is 4 °C/100 m, the trend of the temperature variation in the core chamber during lifting is shown in Fig. 7. The ambient temperature gradually decreases, causing the temperature difference inside and outside the chamber to increase progressively, and the cooling rate inside the chamber gradually accelerates. The average heat dissipation power is 145.8 W with insulation materials present. When the core reaches the ground at 20.8 min, the instantaneous heat dissipation power peaks at 279.2 W. Meanwhile, a significant difference in the core temperatures with and without thermal insulation materials was observed. However, the core temperature will still drop substantially in the presence of thermal insulation materials. Therefore, there is a considerable need to develop deep rock ITP-Coring technology based on the research of temperature preservation through the coupling of active and passive approaches. Theoretical results can also serve as the basis for informing the design of temperature-preservation control modules and energy systems.

In active temperature-preservation design, the temperature sensor and proportional-integral-derivative (PID) chip perform a series of collection-feedback-control actions on the core temperature and ultimately maintain the core temperature by active preservation via graphene heating materials. Tests have been performed on active temperature preservation using graphene heating materials. The corresponding results are shown in Fig. 8. According to the design of the temperature-preservation system of the corer, the materials heat the thermal conductive oil to 150 °C, and the PID chip maintains the oil temperature at 150 °C for 25 min, with slight fluctuations around the target temperature, achieving a control accuracy of 0.97%. The test results show that the combination of graphene heating and a control module effectively controls and accurately measures temperature.

For passive temperature preservation, performance tests of thermal insulation materials and pre-engineering experiments were carried out. Fig. 9 shows the optimization test results of the thermal insulation performance of materials. Among the materials, C1 shows a better thermal insulation effect, which minimizes the internal disturbances resulting from the external temperature variations and reduces the drop in the *in-situ* temperature of the core, making it an appropriate candidate for passive insulation materials in ITP-Coring operations.

To adapt to a high hydrostatic pressure at depth, we innovatively proposed the use of high-pressure-resistant thermal insulation

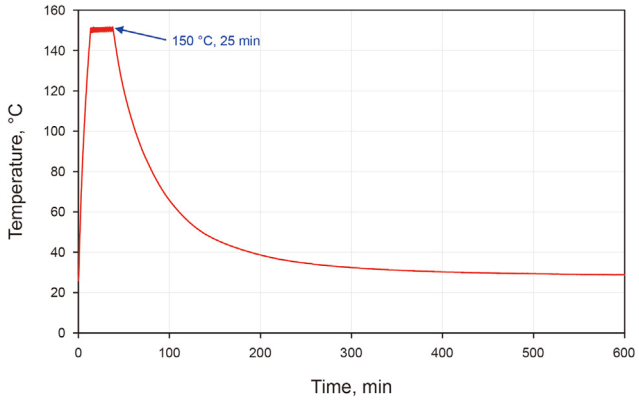

Fig. 8. Test results of active thermal preservation.

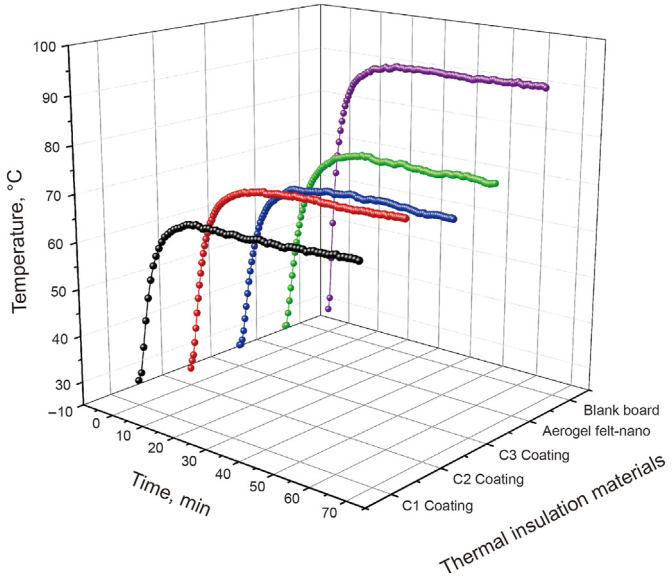

Fig. 9. Optimization results of the heat insulation performance of materials (3 mm and 150 °C).

materials. Tests results verify that these materials can be suitable for hydrostatic environments with pressures up to 40 MPa, and we continue to tackle key problems.

3.1.3. *ISP-, IMP- & ILP-Coring*

In 2018, we first proposed the fundamental principles and technological implementation of ISP-, IMP- and ILP-Coring through the process of *in-situ* solid film forming (Xie et al., 2018a, b). On this foundation, self-adaptive phase transfer film formation and an *in-situ* crosslinking/curing film-forming mechanism and methodology have been proposed (Xie et al., 2020a, b, c). Additionally, Liu et al. (2021) attempted to use the same methodology for coring in old wells. In previous studies (Xie et al., 2020b), we mainly focused on the exploration of the *in-situ* crosslinking/curing film-forming mechanism to realize deep ISP-, IMP- and ILP-Coring. Achieving such an idea relies on the *in-situ* self-curing film forming and adequately covering the rock sample surface. Here, the relationship between the comprehensive performance of the sealing film and its morphological structure formed during coring is introduced. In-depth discussions on the film formation mechanism, material formula, structure, etc., are presented to optimize the applicational properties of the film material.

The principal formation process of the self-curing film is shown in Fig. 10. Prior to the actual coring step, the coring device is filled with liquid A (Fig. 10a). When core drilling procedures, the inner tube space of the corer will be occupied by the rock sample, and then liquid A uniformly coats the surface of the rock sample while pushing it outward so that it is immersed in the fluid. The process actively avoids contamination of the core by the drilling fluid (Fig. 10b). Liquid B is then injected into the corer when the core is lifted upward; when liquid B mixes with liquid A, the crosslinking agent in liquid A starts to cause a rapid crosslinking and curing reaction of the polymer chains, forming a polymeric film with excellent barrier properties (Fig. 10c and d). The key to controlling this process is the rapid sealing of the film-forming solution that achieves effective barrier properties and excellent anti-disturbance capability of the film. Hence, considerable effort has been devoted to exploring the curing time, barrier properties, and mechanical properties of sealing films.

This paper first explores the crosslinking and curing ability of the sealing film. The curing process consists of multiple steps, including hydrolysis of the crosslinking agent and *in-situ* condensation of the polymer matrix. The temperature and catalyst have a significant impact on the crosslinking and curing process. We showed two main conclusions as follows: (1) The crosslinking curing time is reduced significantly by increasing the catalyst content (as shown in Fig. 11a). At 80 °C, the curing time without a catalyst was 115 min. When 0.25 wt% catalyst was added, the curing time was reduced to 30 min. The underlying mechanism is that the −Sn catalyst combines with more affinitive hydroxyl oxygen in the crosslinking agent to form a complex transition state, reducing the activation energy of the reaction to accelerate the curing reaction. (2) The curing time shortens significantly when increasing the temperature (as shown in Fig. 11b). At a catalyst content of 0.25 wt %, the film's curing time is reduced from 88 min at 25 °C to 19 min at 200 °C. We suggest that an increase in temperature greatly promotes mass transfer in the polymer film and its interactions with water vapor. Meanwhile, scanning electron microscopy (SEM) analysis of the film cross-sections (cured within 30 min) showed that the sealing films were dense and compact at the micrometer scale, laying the foundation for achieving the mechanical and barrier property requirements for drilling.

We further incorporated 2D nanosheet fillers with various surfactant modifications to tune the microstructure and lipophilicity of the composite materials in the hope of optimizing the barrier and mechanical properties of the film. We found that the ion exchange reaction between the cationic surfactant and Na^+ in the lamellar filler caused the interlayer spacing to expand (as shown in Fig. 12a). Such an organic filler exhibits an excellent thermal stability that it will not degradation until 225 °C (Zhao et al., 2020). We showed that expanded and exfoliated nanofillers are conducive to constructing tortuous paths for gas diffusion, reducing the permeability of the film and achieving excellent substance- and moisture-preservation properties. When testing the oxygen and water vapor permeability of films with different filler contents, we found that the introduction of lamellar fillers significantly improved the barrier performance. Adding 32 wt% of the fillers into the pure polymer reduced the oxygen and water vapor permeability by 81% and 84%, respectively (see Fig. 12b). The use of lipophilic alkyl chain-

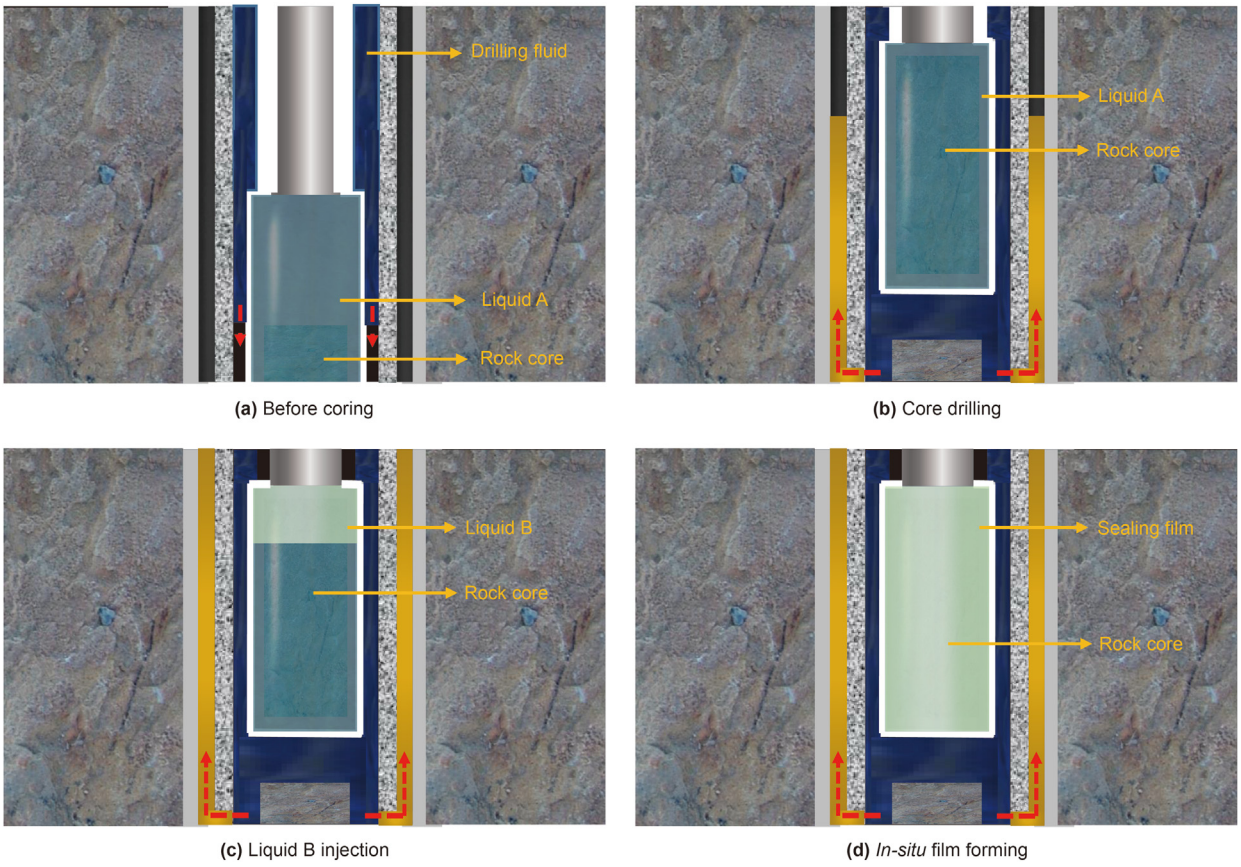

Fig. 10. Schematic diagram of the film-forming process while drilling.

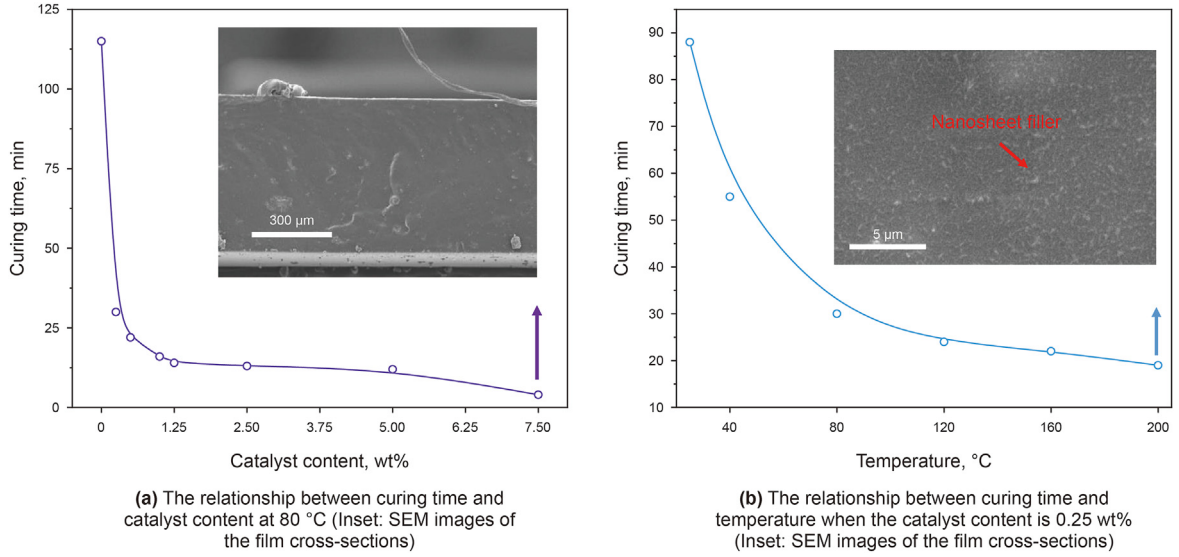

Fig. 11. Study of crosslinking and curing ability.

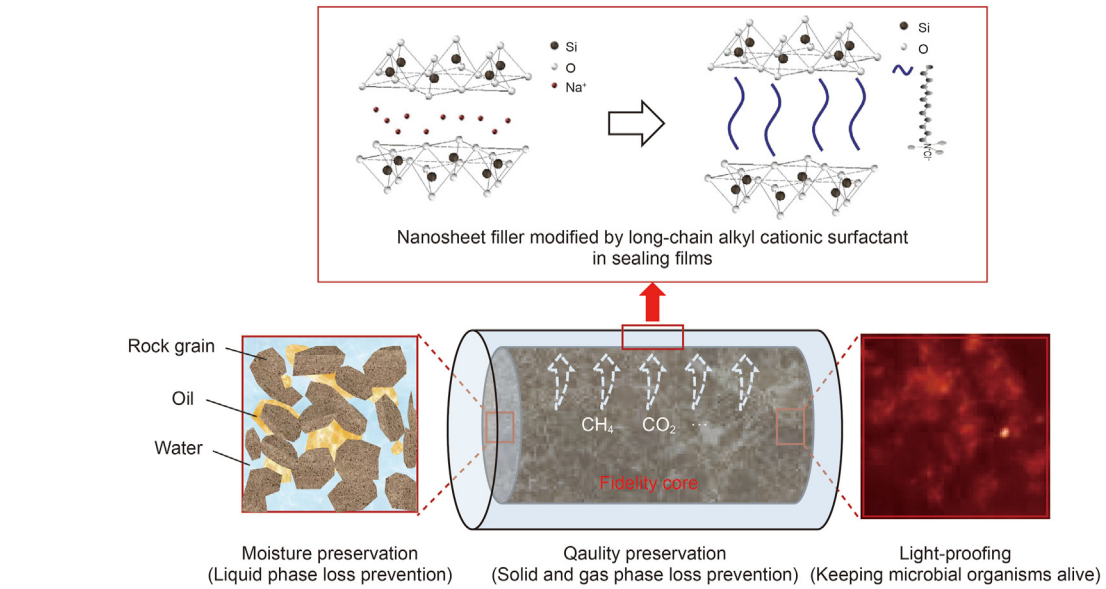

(a) Schematic diagram of the principle of achieving light-preserved and substance and moisture preservation using composite nanofiller sealing film

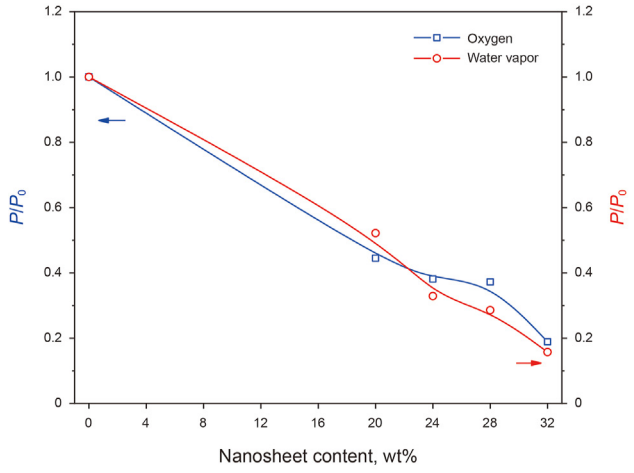

(b) Permeability of water vapor and oxygen with different nanosheet filler contents

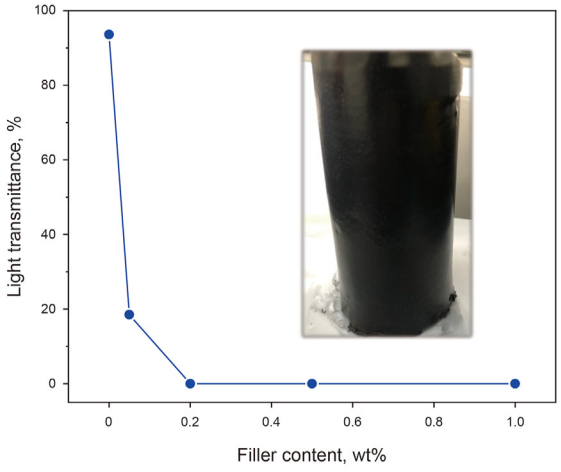

(c) Light transmittance of the substance-preserving film with different filler contents

Fig. 12. Substance and moisture preservation results and light-preserved properties of the sealing films.

Table 1
Testing on mechanical properties of sealing films.

	Elongation at break, %	Tensile strength, MPa
1st	140	0.43
2nd	166.7	0.6
3rd	133	0.43
4th	170	0.63
Average	152.4	0.52

modified lamellar fillers in this study further enhanced the interaction with the matrix so that the fillers were uniformly dispersed in the matrix, ensuring excellent and stable film stretchability and mechanical strength. The material provided strong protection against mechanical disturbance during the core extraction process. As shown in Table 1, the average tensile elongation at break of the sealing film was 152.4%, and the average tensile strength was 0.52 MPa. Additionally, the light transmittance was reduced to 0% by incorporating light-absorbing filler, achieving complete visible-light shielding for the rock sample (as shown in Fig. 12c).

To verify the substance preservation effectiveness of the sealing films in a complex environment, this study further explored the permeability of sealing films in various gases and acid-alkali liquid environments. We tested the permeability of different gases in the film in an independent gas permeability detection device, as shown in Fig. 13a. The N_2 carrier test gas was introduced from one side of the film, and gas chromatography was used to sense the gas concentration on the other side. The gas permeation through the film was recorded when the concentration approached a constant. The

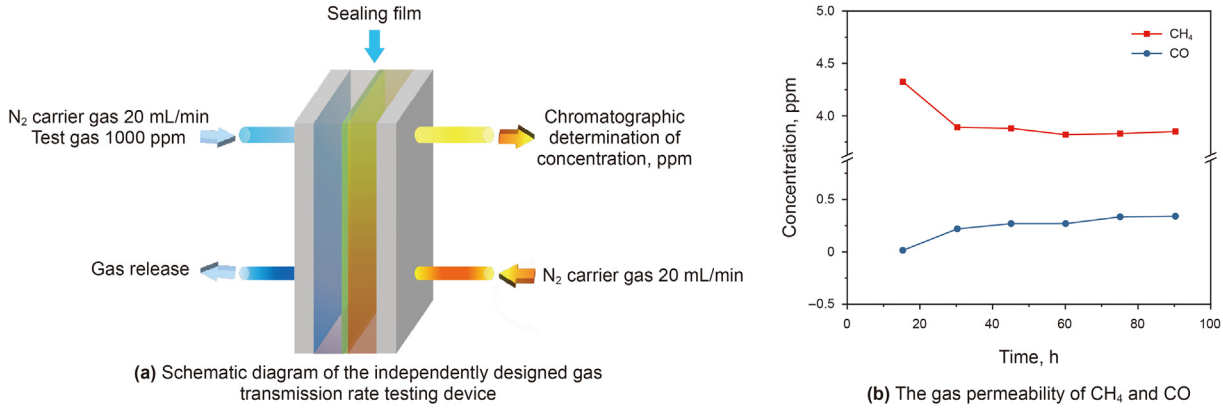

(a) Schematic diagram of the independently designed gas transmission rate testing device

(b) The gas permeability of CH_4 and CO

Fig. 13. One side of the film is filled with nitrogen carrier gas and testing gas, and the other side is filled with nitrogen carrier gas. The testing gas will penetrate to the other side of the film over time and be detected as nitrogen enters the chromatography. The CO and CH_4 permeability of sealing film can be considered as the stable concentration of testing gas.

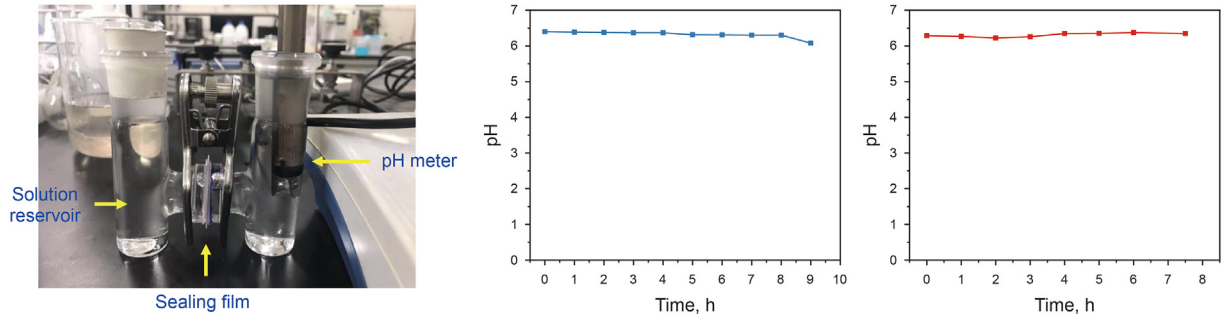

(a) Schematic diagram of the independently designed acid-alkali permeability testing device

(b) Permeability test results for the acidic environment

(c) Permeability test results for the alkaline environment

Fig. 14. Permeability tests in the acidic and alkaline environments.

results showed (Fig. 13b) that the permeability of the film to CH_4 and CO was low, at 3.85 and 0.33 ppm/min, respectively. This is because the film was compounded with nanosheet fillers, which substantially reduced the gas permeability. Meanwhile, this study also examined the barrier properties against different acids and alkali ions with an ion detection device, as shown in Fig. 14a. With acid or alkali solution on one side of the film and distilled water on the other, the pH concentration of the distilled water was measured over a long period of time to determine the permeation. The results showed that the film exhibits excellent properties and stability in both acidic and alkaline environments. With a H_2SO_4 solution at pH = 2 or a NaOH solution at pH = 13 in solution reservoir, the pH meter detected that there was no significant change of pH value on the other side of the membrane (Fig. 14b and c). This pattern is due to the highly crosslinked molecular structure of the sealing film, which makes the film resistant to swelling and inhibits ion transport. Additional benefits arise from the composite nanofiller, which resists water and ion penetration and thereby reduces the ion permeability.

3.2. Research on deep in-situ transfer and storage systems

Deep *in-situ* transfer and storage systems mainly have two functions: (1) reconstructing the *in-situ* environmental conditions, i.e., creating pressure and temperature conditions inside the transfer and storage chamber consistent with those in the *in-situ* environment of the core samples, to ensure that the integrity of the *in-situ* mechanical properties of the deep-occurring rock formation remains intact during the process of transfer and storage; and (2) docking with the corer to transfer the core from the corer to the transfer chamber for storage or to the testing chamber for core testing. One structural design of a deep *in-situ* transferring storage system was established. Studies of the *in-situ* environmental reconstruction method based on temperature and pressure decoupling control were carried out, which preliminarily verified the effect of temperature and pressure control through experiments.

3.2.1. Design of in-situ transfer and storage systems

The *in-situ* sample transfer and storage system consist of a transfer and storage chamber, a docking chamber, a push rod chamber, a transfer device, a sealing structure, and a temperature and pressure control system. Simulations of deep *in-situ* environmental conditions with a high temperature at 150 °C and a high pressure of 140 MPa were achieved in all chambers. Under such a high-temperature and ultrahigh-pressure environment, the designs of the chamber structure, docking device, transfer device, sealing device, and temperature and pressure control were exceptionally challenging.

This study describes the design of the *in-situ* sample transfer

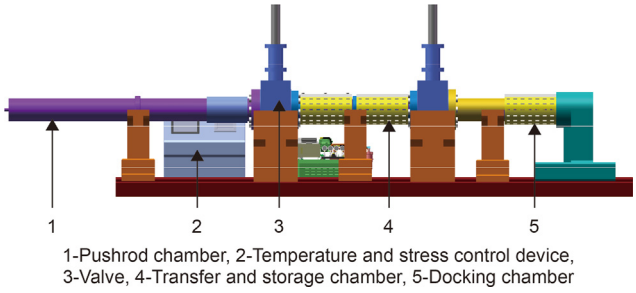

Fig. 15. Architecture of the sample transfer and storage system.

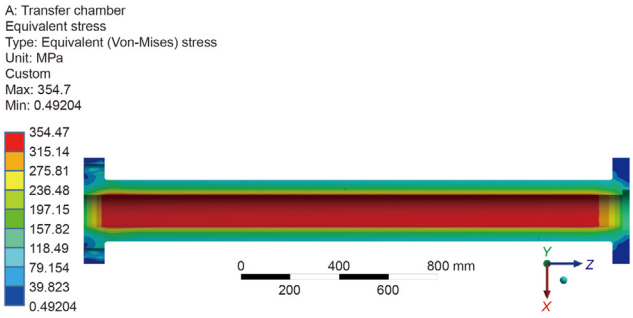

Fig. 16. Chamber stress under a pressure of 140 MPa.

and storage system and the structure of each ultrahigh-pressure chamber. Fig. 15 shows a schematic diagram of the structure of the sample transfer and storage system. The docking chamber was designed so that the corer can go inside it, which allows integrated docking of the transfer and storage chamber and the corer. The dual-circuit hydraulic system made automatic grabbing and transferring of the core possible.

To ensure the structural strength, the designs of all the ultrahigh-pressure chambers comply with the TSG 21–2016 "*Supervision Regulation on Safety Technology of Stationary Pressure Vessels*" standard and adopt a single-layer hollow cylindrical structure. The chamber bodies were built with 20MnNiMo steel, a material with high strength and excellent malleability that is suitable for the manufacture of ultrahigh-pressure vessels. Fig. 16 shows the stress distribution of the *in-situ* transfer and storage chamber under an internal pressure of 140 MPa; the maximum stress was 341 MPa, which met the strength requirements.

3.2.2. Design for reconstruction of in-situ environmental conditions

The reconstruction of *in-situ* environmental conditions was achieved by controlling the pressure and temperature of the fluid in each chamber of the sample transfer and storage system. It was exceptionally difficult to achieve high-precision control of the pressure and temperature due to the following reasons: (1) when heating or cooling at a constant volume, the pressure of the fluid changed with the change in temperature, that is, the high-temperature and high-pressure environment was coupled with the temperature and pressure of the fluid, which increased the difficulty of temperature and pressure adjustment; (2) the opening and closing of the docking valve caused changes in the volume of the fluid inside the transferring storage chamber, which resulted in sharp pressure fluctuations that made pressure control more difficult; and (3) the transfer and storage system had a complex structure, making it difficult for proper placement of the heating device, resulting in an uneven heating distribution in the chamber, which affected the uniformity of the internal temperature field, further challenging temperature control.

The *in-situ* environmental reconstruction system adopted a two-layer control structure. As shown in Fig. 17, the central controller was used to achieve temperature and pressure decoupling control, and the temperature and pressure control targets after decoupling were taken over by the temperature controller and pressure controller, respectively, to be controlled independently.

Fig. 18 shows a schematic diagram of the water temperature and pressure decoupling control path, where curves *AC*, *DE*, and *FG* are all sections of the temperature-pressure curve of water with a constant volume.

Let the initial state of a specific *in-situ* environmental reconstruction be A (P_A, T_A) and the reconstruction targets be B (P_B, T_B). Without affecting the nature of the problem, it can be assumed that

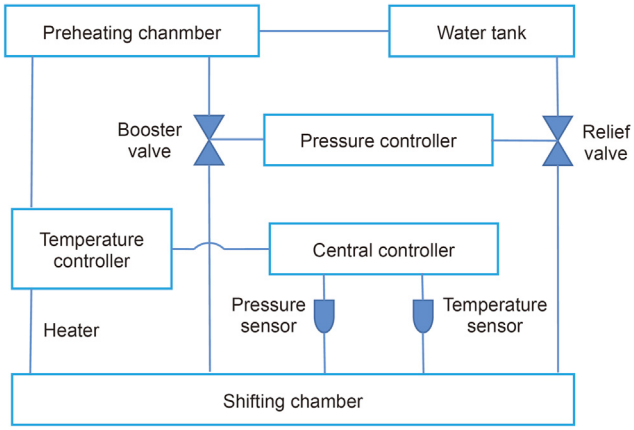

Fig. 17. Schematic diagram of the reconstruction of the deep *in-situ* environmental conditions.

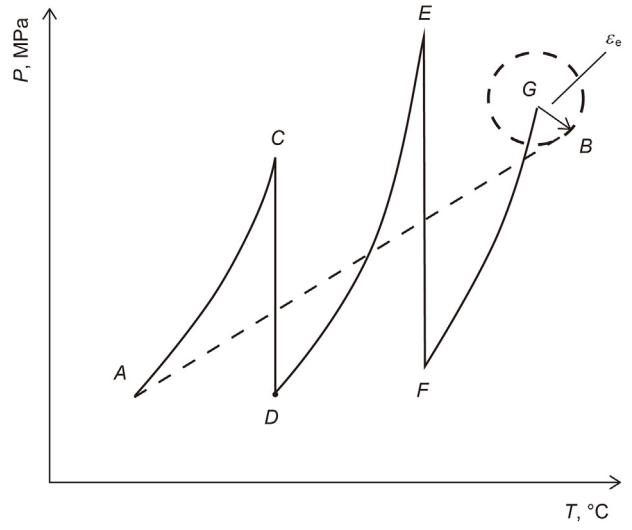

Fig. 18. Water temperature and pressure decoupling control path.

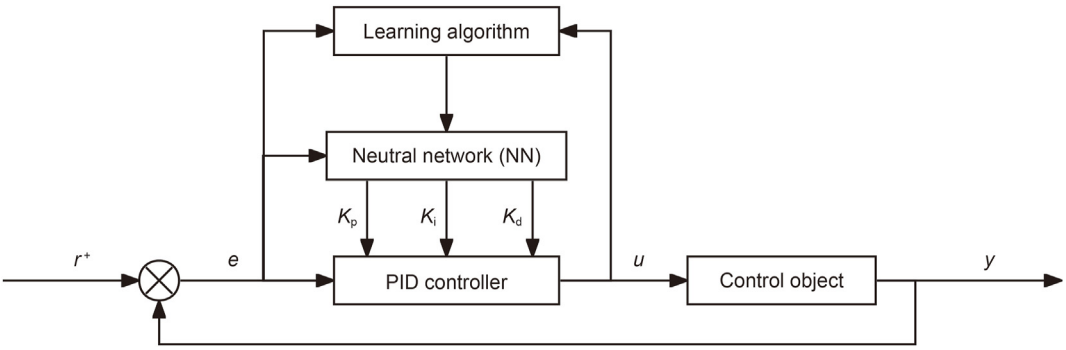

Fig. 19. Structural diagram of a PID pressure and temperature control system based on a neural network.

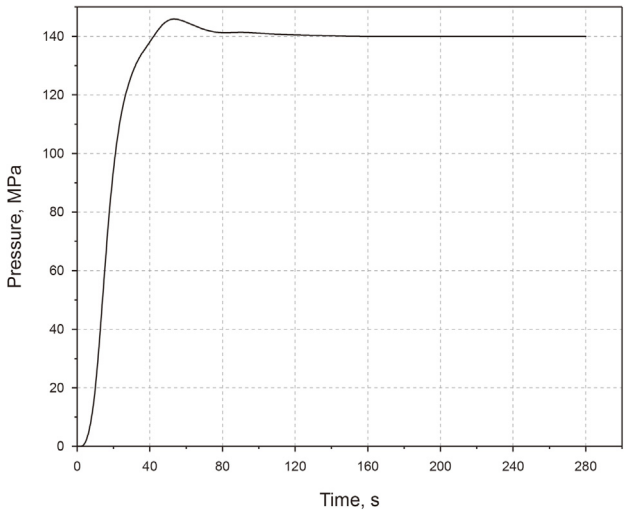

Fig. 20. Test result of the pressure control system.

point *A* is on the isovolumetric temperature-pressure curve in the liquid phase zone. The dotted straight line *AB* represents an ideal temperature and pressure control path; however, control along this straight line is a temperature-pressure coupling control. This paper proposes an interpolation decoupling algorithm for the ideal straight path *AB* to achieve decoupled control of temperature and pressure. First, the temperature is raised to point *C* along the isodensity curve *AC* from point *A*, and then the pressure is released to point *D* while maintaining the temperature; the curve *AC* and the straight line *CD* constitute an interpolation. This interpolation process is repeated until point *B* is reached.

Intermediate interpolation points such as *C* and *D* are controlled by the intermediate temperature and pressure error threshold ε_m; a smaller ε_m can be assumed to minimize temperature and pressure fluctuations in the adjustment process, while a larger ε_m can be assumed if the number of interpolation steps is to be reduced to improve the control efficiency. The interpolation endpoint *G* is controlled by the terminal temperature and pressure error threshold ε_e.

The curved path *AC* and straight path *CD* are independent temperature and pressure control paths, respectively, making decoupled control possible. To avoid temperature disturbance caused by the medium injection during the pressurization adjustment, a preheating chamber synchronized with temperature control is used to achieve medium preheating.

Given the large inertia and nonlinear characteristics of the pressure and temperature control system presented in this paper, a PID pressure and temperature control algorithm based on neural networks was designed to control the decoupled temperature and pressure. Fig. 19 shows the structural diagram of this control system. The pressure control system was divided into three parts: (1) the pressure signal acquisition module; (2) the signal processing and pressure control module; and (3) the host computer communication module. A single-chip microcomputer was used as the central controller for pressure control, and the booster device was a high-performance pneumatic booster pump.

Fig. 20 shows the pressure change curve when the PID control method based on neural networks was adopted. The pressure response was quick, the system was stable, and the steady-state error was less than 1%.

The temperature control system used an integrated heating device consisting of a distributed copper heating jacket and a heat-conducting serpentine oil tube, as shown in Fig. 21; on this basis, the design verified the PID temperature control algorithm based on

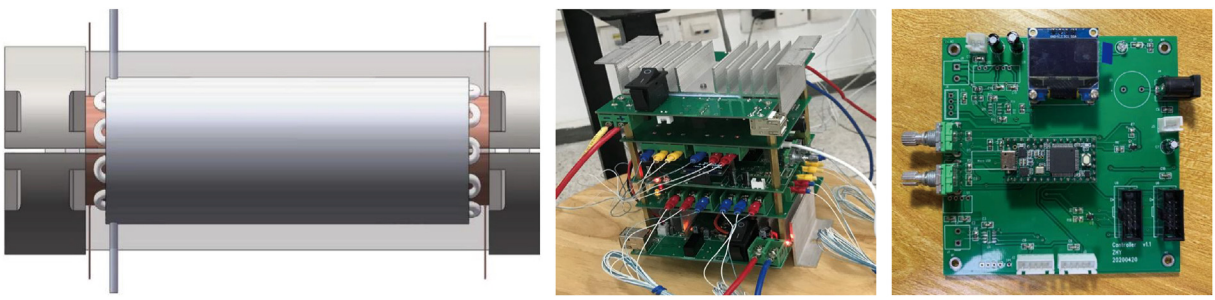

Fig. 21. Heating device of the transfer and storage chamber.

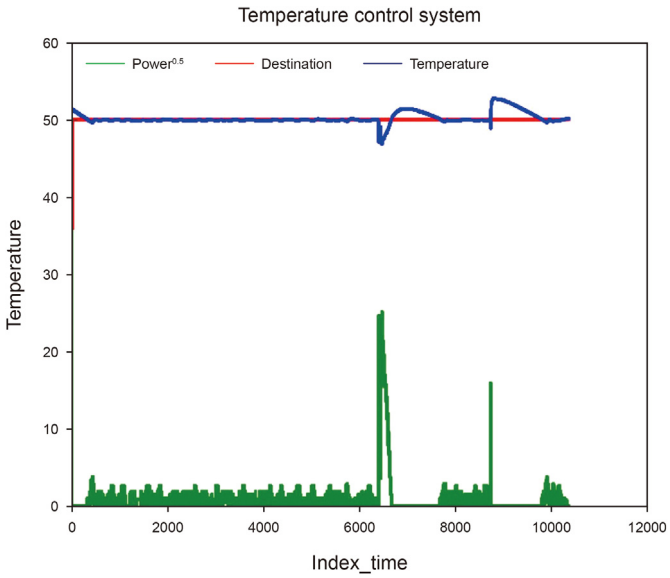

Fig. 22. Temperature control test results.

neural networks. Fig. 22 shows the temperature control test results, where the red line represented the target temperature, the blue line was the actual temperature, and the green line was the disturbance applied on the system. The steady-state temperature error was ±0.2 °C, and the stabilization time was 2 s when there was disturbance.

3.3. Research on testing systems in simulated deep in-situ environment

The deep *in-situ* mechanical testing system used here obtains the most accurate physical and mechanical properties of deep rocks via noncontact acoustic, electrical and magnetic tests. The test samples were prepared through high-precision cutting in the reconstructive environment, and the mechanical response and characteristics of the deep rocks were revealed. Presently, noncontact testing, rock sample preparation, and mechanical testing under *in-situ* conditions remain technical challenges worldwide.

This deep *in-situ* testing system consists of noncontact acoustic, electrical, and magnetic physical testing modules, a sample preparation module, a loading test module, and a data analysis module. The system provides the following functions: (1) noncontact acoustic, electrical, and magnetic sensors are used to obtain the rock physical properties of wave velocity and pore structure in a deep simulated environment; (2) a diamond wire cutter is used to prepare samples via a standard core preparation process with only small temperature and mechanical disturbances; and (3) the deformation and failure properties of deep *in-situ* rock masses are obtained through real-time loading of *in-situ* rock cores.

3.3.1. Design of noncontact testing systems for use in in-situ environments

The goal of the noncontact testing system design and sample preparation system are to maintain the integrity of the *in-situ* core parameters, such as core density, resistivity, porosity, and sonic velocity. In the reconstructed *in-situ* environment, standardized samples are prepared with low-damage, low-disturbance, and high-precision cutting and preparation processes. A high-precision control mechanism was developed to perform translation, rotation, and cutting under a unique environment with a high temperature and high pressure. Ultimately, a noncontact testing and sample preparation system for a deep *in-situ* environment was constructed.

An acoustic wave testing subsystem with the “one transmitter vs. multiple receivers” working mode was established and could measure the wave velocity and elasticity modulus. The electric testing subsystem with the “one transmitter vs. multiple receivers” working mode was created based on the principle of direct current electrodes, which could be used to obtain the internal resistance distribution, porosity and moisture content of the rock through the excitation voltage of the external host of the testing chamber. An innovative magnetic field coil arrangement was designed based on the principle of the transient electromagnetic method, and a magnetic testing subsystem with the “one transmitter vs. multiple receivers” working mode was created, which emits a pulsed magnetic field via a magnetic source, receives the response magnetic field of the rock core in the chamber, and calculates the water, oil, and gas contents. The design of the noncontact testing system is shown in Fig. 23.

Measurement experiments using noncontact acoustic waves were preliminarily completed. During the experimentation, three types of sensors were designed: a pure metal sensor testing ring, a metal sensor testing ring cushioned with polymer, and a low-density polymer sensor testing ring. Basic noncontact acoustic wave tests under normal temperature and pressure conditions were performed in groups.

The results are shown in Tables 2–4. The results show that compared with the contact testing results, 36% errors were recorded by the pure metal sensor testing ring, and errors greater than 40% were recorded by the metal sensor testing ring cushioned with polymer. In the situation where the low-density polymer was used as the sensor test ring material, the errors recorded by the low-density polymer sensor testing ring were less than 6% than the contact test results. In comparison, the noncontact acoustic wave test results using a low-density polymer as the ring sensor holder

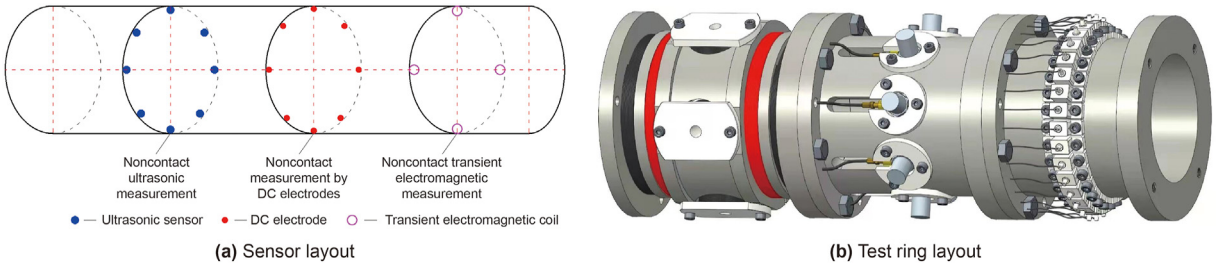

Fig. 23. Schematic diagram of the noncontact system design.

Table 2
Test results of scenario I.

Sample	Diameter, mm	Height, mm	Contact		Noncontact	
			Time difference, μs	Wave velocity, m/s	Time difference, μs	Wave velocity, m/s
Granite	47.5	100.30	9.1	5277.78	13	3653.85
Siltstone	49.2	100.20	11.0	4472.72	17	2894.11
Medium sandstone	49.4	99.70	26.0	1900.00	32	1543.75
Hydraulic oil	Test probe distance: 55		38,0	1447.36	–	–

Table 4
Test results of scenario III.

Sample	Diameter, mm	Height, mm	Contact		Noncontact	
			Time difference, μs	Wave velocity, m/s	Time difference, μs	Wave velocity, m/s
Granite	47.5	100.30	9.5	5000.00	10.1	4702.97
Siltstone	49.2	100.20	9.0	5466.67	9.2	5347.82
Medium sandstone	49.4	99.70	19.0	2600.00	20.4	2421.56
Hydraulic oil	Test probe distance: 55		38.0	1457.2	–	–

Table 3
Test results of scenario II.

Sample	Diameter, mm	Height, mm	Contact		Noncontact	
			Time difference, μs	Wave velocity, m/s	Time difference, μs	Wave velocity, m/s
Granite	47.5	100.30	9.2	5163.04	16.0	2968.75
Siltstone	49.2	100.20	10.1	4871.28	16.0	2971.50
Medium sandstone	49.4	99.70	22.0	2245.45	36.0	1347.25
Hydraulic oil	Test probe distance: 55		38.0	1447.36	–	–

material were basically consistent with the contact acoustic wave measurement results.

3.3.2. Sample preparation for testing in simulated environment

There are two types of standard rock samples required for *in-situ* testing: cylindrical samples ($\phi 50 \times 100$ mm) and cubic samples ($30 \times 30 \times 30$ mm^3). The rock sample preparation system installed in the simulated *in-situ* environmental reconstruction chamber comprises two modules: the cylindrical sample preparation module and the cubic sample preparation module.

3.3.2.1. The cylindrical sample cutting mechanism. For cylindrical sample preparation, the parallel cutting of the two end faces is key. The sample cutting is completed by the relative movement of the diamond saw blade and the rock sample in the *in-situ* environment. The transferring mechanism fixes the core, and the fine cutting of the axial cross-section of the rock sample is completed by vertically lifting the wire winding wheel. Compared with other cutting methods, this is the preferred method for rock sample preparation in a simulated environment. It minimizes the impact on the integrity of the original core information, controls the flatness and parallelism of the rock cutting surface with high precision, has excellent working durability and stability, and is capable of achieving low-disturbance and high-precision preparation and control of samples in a simulated *in-situ* environment. The design of the cylindrical sample cutting mechanism is shown in Fig. 24.

3.3.2.2. The cubic sample cutting mechanism. The preparation of cubic samples in the *in-situ* environment requires six-sided cutting of the core, in which the cylindrical samples require cutting the two cross-sections in the vertical axis, the cylindrical sample is then moved along with the axis by the transferring mechanism, the two pairs of vertical slitting mechanisms installed along the axial direction successively cut out four sections as the cylindrical core advances along the axial direction, thereby obtaining cubic samples for testing. The design of the cutting mechanism for cubic rock samples is shown in Fig. 25.

3.3.3. Design of the loading test system

Loading tests in a deep *in-situ* environment were carried out to study the mechanical behavior of deep *in-situ* rock samples. The subsystem adopts a separable structure consisting of a high-precision triaxial testing machine and a high-fidelity triaxial loading test chamber. The loading test chamber can be joined with the above-mentioned rock sample preparation chamber and separated after the sample being transferred, which is then moved to the triaxial testing machine for further experimental studies. The triaxial testing machine handles loading and unloading control under various complex conditions and conducts real-time monitoring and analysis of the process from deformation to failure of the rock samples.

3.3.3.1. The triaxial load testing machine. The high-precision triaxial testing machine provides triaxial loading and unloading control for testing rock samples in an *in-situ* environment and real-time measurement of various signals. The system composition module is shown in Fig. 26, which mainly consists of a host, some sensors and transmitters, high sensitivity electro-hydraulic servo controller, hydraulic source, cooling machine, temperature control system, and system control software.

The host consists of a high-rigidity frame and three groups of dynamic servo pistons precisely mounted to it in three orthogonal

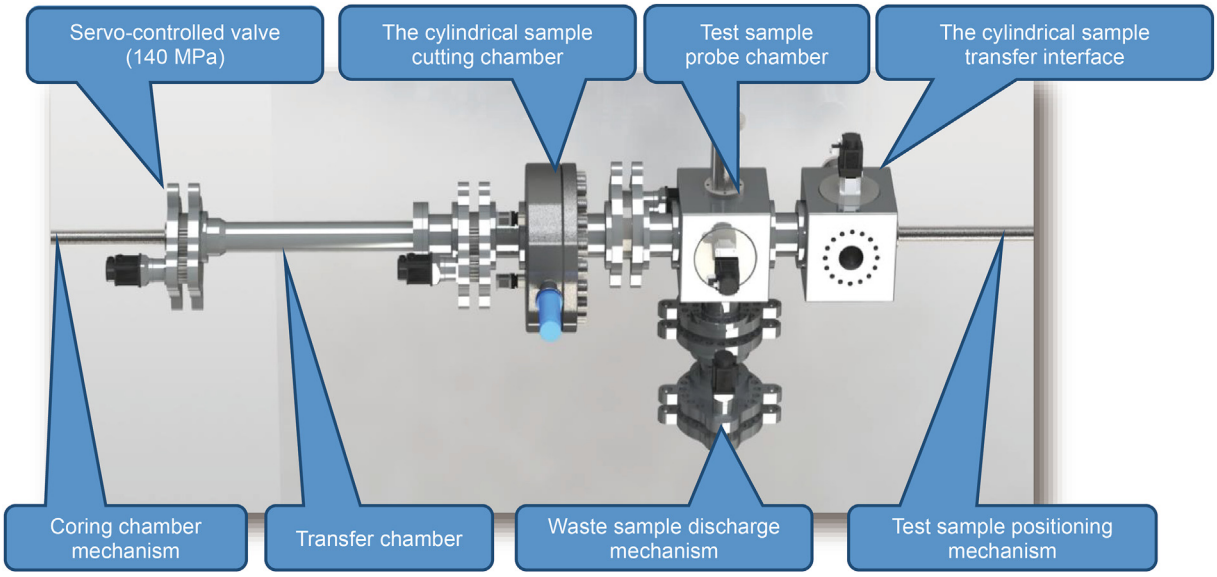

Fig. 24. Schematic diagram of the design of the cutting mechanism for cylindrical rock samples.

directions. The loading test chamber can be accurately placed between the cylinder pistons with the clamping and positioning device on the host. The cross-sectional area of the frame is maximized by using a large-cross-section cylinder to improve the rigidity of the host, guaranteeing the measurement of the full load-displacement curve of the rock sample.

The electrohydraulic servo controller should meet the requirements for high sensitivity with large-flow dynamic regulation to achieve accurate loading and unloading servo control. Then, the independently designed high-precision device powered by oil is capable of accurately simulating the ground stress levels of different depths, and the maximum axial load can reach 1500 kN. The temperature control device with a maximum temperature capacity of 150 °C can maintain the core temperature closing to the *in-situ* temperature of deep rock, which fully meets the requirements of testing. With the help of the seepage control system, 140 MPa of pressure can be provided during testing to simulate the high-pressure conditions at depth, thereby facilitating the stress-temperature-seepage field coupling testing.

3.3.3.2. The triaxial loading test chamber. For cubic samples, the high-fidelity triaxial loading test chamber is composed of a chamber at a high temperature and pressure and with six piston rods and indenters. The indenters at the ends of the six piston rods contact the six surfaces of the sample, providing true triaxial loading in six directions. Multiple acoustic emission positioning probes embedded in the indenters can accurately determine the location of failure and fractures, as shown in Fig. 27.

For cylindrical samples, the loading test chamber is composed of a chamber at a high temperature and high pressure with an annular oil bag, two piston rods and indenters. The indenters of the two piston rods provide a constant axial load, and the annular oil bag is used to apply an adjustable confining pressure to achieve pseudo triaxial loading. Several displacement sensors and acoustic emission positioning probes are attached on the inner wall of oil bag or embedded in the indenters to perform real-time monitoring of the deformation and fracture of the samples, as shown in Fig. 27. The pseudo triaxial loading test chamber can be used with a variety of testing machines that is now available to complete the loading, and

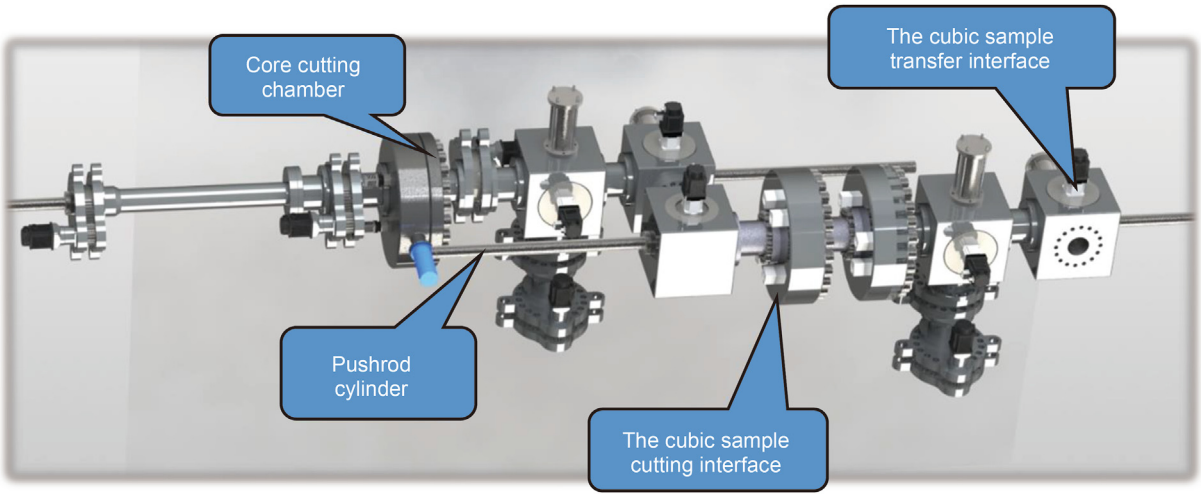

Fig. 25. Schematic diagram of the cutting mechanism design for cube rock samples.

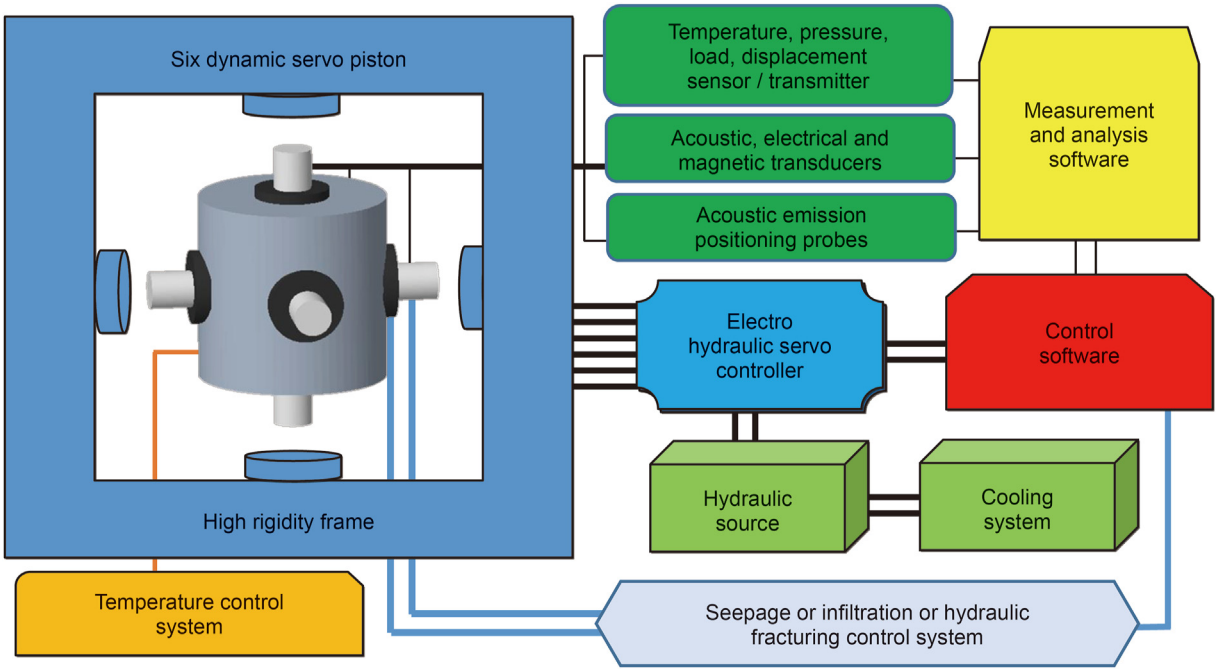

Fig. 26. Composition block diagram of the high-precision triaxial testing system.

it can also be used with the aforementioned true triaxial testing machine to complete the loading in one direction, which also improves the system flexibility and fully reflects the advantages of the separable structure.

The precise joining between the loading test chamber and the above-mentioned rock sample preparation chamber is the key to ensuring sample alignment and transfer. This can be achieved by an accurate transferring system and a joining valve. First, the preparation chamber and the loading test chamber are connected through the valve, the valve is opened after pressurization, the sample is pushed from the preparation chamber to the loading test chamber by the electric push rod, the chamber is then sealed to preserve pressure, and finally the loading chamber is disconnected and removed. The chamber with the sample can then be moved to the testing system.

The loading and testing system can reconstruct the deep *in-situ* environment and simulate various loading and unloading paths for conducting integrated testing and analysis of rock mechanics under multifield and multiphase coupling conditions. The loading test chamber is equipped with multiple sensors, providing a signal transmission channel for the system. Through servo control, the simulated *in-situ* environment can be maintained. The stress, strain, and pore pressure changes during rock deformation and failure can also be comprehensively detected during experiments. Various acoustic, electrical, and magnetic sensors are used to measure and characterize the energy dissipation and release, and

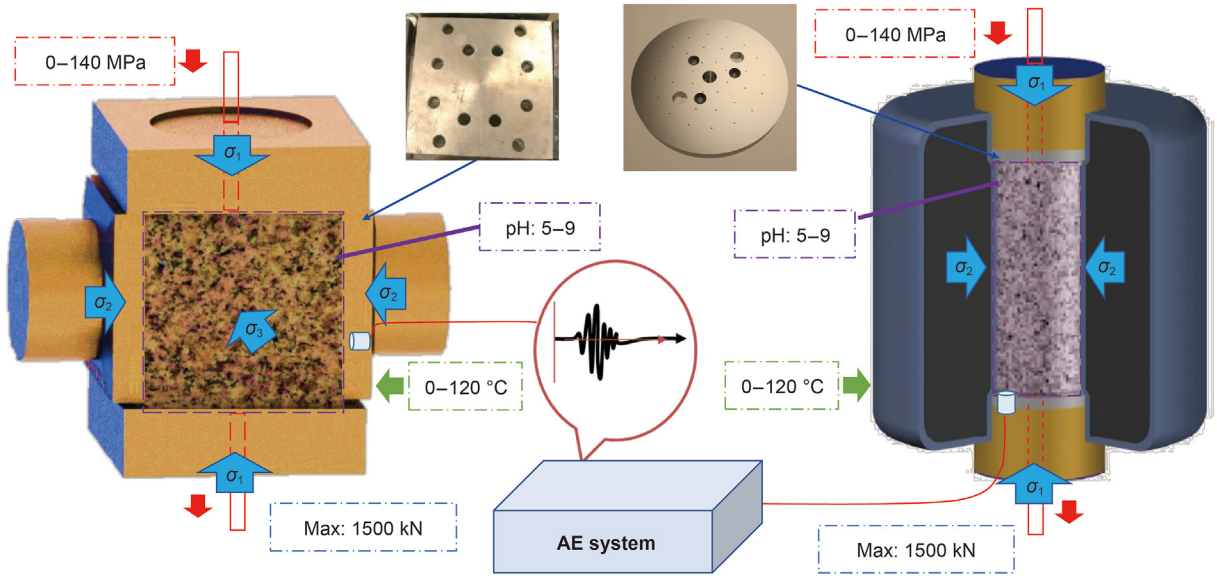

Fig. 27. Schematic diagram of rock sample loading tests in the simulated environment.

acoustic CT technology can be further employed to determine the distribution of the microcracks and even macrocracks and obtain multisource information to build a database that fully reflects the mechanical response of rock. With this testing system, it is possible to study the transition between the elastic and plastic states of deep rock and the change in the failure mechanism under multiphase and multifield coupling conditions in reconstructed deep *in-situ* environments to reveal the law of multifield coupling and establish a multiphase and multifield coupling theory of deep resource mining.

4. Conclusions and prospects

To obtain samples from the deep earth and research the mechanical properties of deep *in-situ* rocks, this paper is the first to propose the concept of ICP-Coring and testing systems for deep rock, including an *in-situ* coring, storing and transferring system and a testing system, have been developed. The main conclusions can be summarized as follows:

For deep IPP-Coring, five innovative types of Steinmetz solid pressure controllers were designed. According to the simulation results, the ultimate pressure bearing capacities of controllers A1, A2, and A3 are 27.8, 66.3, and 100.5 MPa, respectively. The D type and E controllers are still capable of effective hermetic sealing at 200 MPa.

In terms of deep ITP-Coring, ultrathin graphene active temperature-preservation technology is proposed. This technology, in combination with passive thermal insulation coating, achieved temperature from room temperature to 150 °C, with an error rate of 0.97%.

In terms of deep ISP-, IMP- and ILP-Coring, the crosslinking/curing ability, substance and moisture preservation performance, light-preserved performance, stretchability, strength, and stability of the film material have been further improved through investigation of the relationship between the comprehensive performance of the material and its morphology and structure. The sealing film can be rapidly formed within 30 min with a dense microstructure. Compared to the pure matrix film, the oxygen and water vapor permeabilities of the sealing film are reduced by 81% and 84%, respectively, by incorporating functional 2D nanosheets, and the light transmittance is reduced to 0%. This film can also stay stabilized in complex environments such as acidic, alkaline, and saline environments, for long periods of time.

The structural design of the noncontact acoustic-electric-magnetic test module under a reconstructed deep *in-situ* environment is presented. The structural concept of the test sample preparation system in an *in-situ* environment is proposed, preliminary investigations of noncontact ultrasonic tests are carried out, and high-precision noncontact measurements of the core wave velocity are achieved.

For the contact testing system, an innovative separable loading test chamber is proposed to preserve simulated in-situ environment. In combination with an independent triaxial testing machine, this chamber can achieve triaxial testing in reconstructed environments.

The above research results are expected to facilitate access to more accurate information on the characteristics of deep *in-situ* rock and the laws of its physical and mechanical behavior, reveal the essential differences in the physical and mechanical behavior of rock between deep and shallow environments, discover new phenomena in deep-earth science, clarify the laws of the physical and mechanical behavior of rocks at different depths under *in-situ* conditions, result in new theories of deep rock mechanics and new methods and technologies for exploring the deep earth, provide theoretical and technical support for the national deep-earth exploration strategy, and provide research methods and technical support for deep resources and space development engineering targeting issues such as the mining of minerals, oil and gas resource development, geothermal development, underground urban construction, disaster prevention and control, deep energy storage, military defense engineering, polar development, and seabed mining.

Declaration of competing interest

The authors declare that they have no known competing financial interests or personal relationships that could have appeared to influence the work reported in this paper.

Acknowledgments

The paper was supported by the Program for Guangdong Introducing Innovative and Enterpreneurial Teams (No. 2019ZT08G315) and National Natural Science Foundation of China (No. 51827901, U2013603, and 52004166).

References

Amann, H., Hohnberg, H., Reinelt, R., 2021. HYACE-A Novel Autoclave Coring Equipment for Systematic Offshore Gashydrate Sampling. Deutsche Wissenschaftliche Gesellschaft für Erdgas und Kohle e.V.

Ashena, R., Thonhauser, G., 2018. Coring Methods and Systems. Springer.

Bohrmann, G., Kuhs, W., Klapp, S., et al., 2007. Appearance and preservation of natural gas hydrate from Hydrate Ridge sampled during ODP Leg 204 drilling. Mar. Geol. 244, 1–14. https://doi.org/10.1016/j.margeo.2007.05.003.

Chen, Y., Qin, H.-W., Li, S.-L., et al., 2006. Research on pressure tight sampling technique of deep-sea shallow sediment–A new approach to gas hydrate investigation. China Ocean Eng. 20 (4), 657–664. https://doi.org/10.3723/ut.33.019, 2006.

Coney, L., Wu, Reimold, Gibson, R.L., et al., 2007. Geochemistry of impactites and basement lithologies from ICDP borehole LB-07A, Bosumtwi impact structure, Ghana. Meteoritics Planet Sci. 42 (4–5), 667–688. https://doi.org/10.1111/j.1945-5100.2007.tb01067.x.

Dell'Agli, G., Mascolo, G., 2000. Low temperature hydrothermal synthesis of ZrO_2–CaO solid solutions. J. Mater. Sci. 35, 661–665. https://doi.org/10.1023/A:1004740830928.

Di Girolamo, G., Blasi, C., Schioppa, M., et al., 2010. Structure and thermal properties of heat treated plasma sprayed ceria-yttria co-stabilized zirconia coatings. Ceram. Int. 36, 961–968. https://doi.org/10.1016/j.ceramint.2009.10.020.

Dickens, G.R., Wallace, P.J., Paull, C., et al., 2000. Detection of methane gas hydrate in the Pressure Core Sampler (PCS): volume-pressure-time relations during controlled degassing experiments. Proc. Ocean Drill. Progr. Sci. Results 164, 113–126. https://doi.org/10.2973/odp.proc.sr.164.210.2000.

Dickens, G.R., Schroeder, D., Hinrichs, K.-U., 2003. The Pressure Core Sampler (PCS) on ODP Leg 201: General Operations and Gas Release. Proceedings of the Ocean Drilling Program, Initial Reports Volume 201.

Friðleifsson, G.Ó., Albertsson, A., Elders, W., et al., 2010. The Iceland deep drilling project (IDDP)–10 years later–still an opportunity for an international collaboration. Proceed. World. Geothermal. Cong. 25–29.

Friðleifsson, G.Ó., Albertsson, A., Elders, W., et al., 2011. The Iceland deep drilling project (IDDP): planning for the second deep well at Reykjanes. Trans. Geothermal. Resources. Council 35, 347–354.

Friðleifsson, G.Ó., Elders, W., Zierenberg, R., et al., 2017. The Iceland Deep Drilling Project 4.5 km deep well, IDDP-2, in the seawater recharged Reykjanes geothermal field in SW Iceland has successfully reached its supercritical target. Sci. Drill. 23, 1–12. https://doi.org/10.5194/sd-23-1-2017.

Fulthorpe, C., Miller, K., Droxler, A., et al., 2008. Drilling to decipher long-term sea-level changes and effects - a joint consortium for ocean leadership, ICDP, IODP, DOSECC, and Chevron Workshop. Sci. Drill. 6. https://doi.org/10.2204/iodp.sd.6.02.2008.

Gao, M.Z., Zhang, R., Xie, J., et al., 2018a. Field experiments on fracture evolution and correlations between connectivity and abutment pressure under top coal caving conditions. Int. J. Rock Mech. Min. Sci. 111, 84–93. https://doi.org/10.1016/j.ijrmms.2018.01.003.

Gao, M.Z., Zhang, Z.L., Xiangang, Y., et al., 2018b. The location optimum and permeability-enhancing effect of a low-level shield rock roadway. Rock Mech. Rock Eng. 51 (9), 2935–2948. https://doi.org/10.1007/s00603-018-1461-x.

Gao, M.Z., Wang, M.Y., Xie, J., et al., 2020a. In-situ disturbed mechanical behavior of deep coal rock. J. China Coal Soc. 45 (8), 2691–2703. https://doi.org/10.13225/j.cnki.jccs.2020.0784 (in Chinese).

Gao, M.Z., Xie, J., Gao, Y.N., et al., 2021a. Mechanical behavior of coal under different mining rates: a case study from laboratory experiments to field testing. Int. J. Mining. Sci. Technol. 31 (5), 825–841. https://doi.org/10.1016/

j.ijmst.2021.06.007.
Gao, M.Z., Xie, J., Guo, J., et al., 2021b. Fractal evolution and connectivity characteristics of mining-induced crack networks in coal masses at different depths. Geomech. Geophys. Geo-energ. Geo-resour. 7 (1). https://doi.org/10.1007/s40948-020-00207-4.
Gao, M.Z., Zhang, J.G., Li, S.W., et al., 2020b. Calculating changes in fractal dimension of surface cracks to quantify how the dynamic loading rate affects rock failure in deep mining. J. Cent. S. Univ. 27, 3013–3024. https://doi.org/10.1007/s11771-020-4525-5.
Gao, M.Z., Liu, J.J., Lin, W.M., et al., 2020c. Study on in-situ stress evolution law of ultra-thick coal seam in advance mining. Coal Sci. Technol. 48 (2), 28–35. https://doi.org/10.13199/j.cnki.cst.2020.02.003 (in Chinese).
Guo, J.C., Zhou, H.Y., Zeng, J., et al., 2020. Advances in low-field nuclear magnetic resonance (NMR) technologies applied for characterization of pore space inside rocks: a critical review. Petrol. Sci. 17 (5), 1281–1297. https://doi.org/10.1007/s12182-020-00488-0.
He, Z.Q., Chen, L., Lu, T., et al., 2019. The optimization of pressure controller for deep earth drilling. Therm. Sci. 23 (Suppl. 3), S877–S885. https://doi.org/10.2298/TSCI180612123H.
He, Z.Q., Xie, H.P., Gao, M.Z., et al., 2020. Design and verification of a deep rock corer with retaining the in situ temperature. Adv. Civ. Eng. 11, 1–13. https://doi.org/10.1155/2020/8894286.
Heeschen, K.U., Haeckel, M., Hohnberg, H., et al., 2007. Pressure coring at gas hydratebearing sites in the eastern Black Sea off Georgia. Geophys. Res. Abstr. 9.
Hodgson, D., Bentley, M., Smith, J., et al., 2016. Technologies for retrieving sediment cores in Antarctic subglacial settings. Phil. Trans. Math. Phys. Eng. Sci. 374. https://doi.org/10.1098/rsta.2015.0056, 2059), 20150056.
Hohnberg, H., Amann, H., Abegg, F., et al., 2003. Pressurized coring of near-surface gas-hydrate sediments on Hydrate Ridge: the Multiple Autoclave Corer, and first results from pressure-core X-Ray CT scans. Geophys. Res. Abstr. 5, 09128, 2003.
Jin, Y., Konno, Y., Nagao, J., 2014. Pressurized subsampling system for pressured gas-hydrate-bearing sediment: microscale imaging using X-ray computed tomography. Rev. Sci. Instrum. 85, 094502. https://doi.org/10.1063/1.4896354.
Kashefi, K., Lovley, D., 2003. Extending the upper temperature limit for life. Science 301, 934. https://doi.org/10.1126/science.1086823.
Khizar, A., Giovanni, S., Catalin, T., et al., 2015. Review of pressure coring systems for offshore gas hydrates research. Underw. Technol. 33 (1), 19–30. https://doi.org/10.3723/ut.33.019.
Kim, S., Lee, M., Lee, K., et al., 2021. Data-driven estimation of three-phase saturation during gas hydrate depressurization using CT images. J. Petrol. Sci. Eng. 205, 108916. https://doi.org/10.1016/j.petrol.2021.108916.
Kvenvolden, K., Barnard, L., Cameron, D., 1983. Pressure Core Barrel: Application to the Study of Gas Hydrates, Deep Sea Drilling Project Site 533, Leg 76. Initial Reports DSDP, Leg 76, Norfolk to Fort Lauderdale. https://doi.org/10.2973/dsdp.proc.76.107.1983.
Lee, J., Schultheiss, P., Druce, M., et al., 2009. Pressure core sub sampling for GH production tests at in situ effective stress. Fire in the Ice 9 (4), 16–17.
Lee, J.Y., Jung, J.W., Lee, M., et al., 2013. Pressure core based study of gas hydrates in the Ulleung Basin and implication for geomechanical controls on gas hydrate occurrence. Mar. Petrol. Geol. 47, 85–98. https://doi.org/10.1016/j.marpetgeo.2013.05.021.
Li, C., Xie, H., Gao, M., et al., 2021. Novel designs of pressure controllers to enhance the upper pressure limit for gas-hydrate-bearing sediment sampling. Energy 227, 120405. https://doi.org/10.1016/j.energy.2021.120405.
Li, S.L., Cheng, Y., Qin, H.W., et al., 2006. Development of pressure piston corer for exploring natural gas hydrates. J. Zhejiang Univ. 40 (5), 888–892. https://doi.org/10.3785/j.issn.1008-973X.2006.05.033.
Litt, T., Krastel, S., Sturm, M., et al., 2009. Lake van drilling project 'PALEOVAN', international continental scientific drilling program (ICDP): results of a recent pre-site survey and perspectives. Quat. Sci. Rev. 28, 1555–1567. https://doi.org/10.1016/j.quascirev.2009.03.002.
Liu, H., Sl, W., Pei, X.H., et al., 2021. Development of in-situ fidelity continuous coring tools for old wells in oilfields. Acta Pet. Sin. 42 (3), 358–366. https://doi.org/10.7623/syxb202103009 (in Chinese).
Man, K., Zhou, H.W., 2010. Research on dynamic fracture toughness and tensile strength of rock at different depths. Chin. J. Rock Mech. Eng. 29 (8), 1657–1663 (in Chinese). https://kns.cnki.net/kcms/detail/detail.aspx?dbcode=CJFD&dbname=CJFD2010&filename=YSLX201008021&uniplatform=NZKPT&v=twlOvu6SzOMYKQ81SFvPdFpBU7w20AcfxtBfFii8bYaIR2sSDPM7JRLkdLgqeW5q.
Milkov, A.V., Dickens, G.R., Claypool, G.E., et al., 2004. Co-existence of gas hydrate, free gas, and brine within the regional gas hydrate stability zone at Hydrate Ridge (Oregon margin): evidence from prolonged degassing of a pressurized core. Earth Planet Sci. Lett. 222 (3), 829–843. https://doi.org/10.1016/j.epsl.2004.03.028.
Nagao, J., Yoneda, J., Konno, Y., et al., 2015. Development of the Pressure-Core Nondestructive Analysis Tools (PNATs) for Methane Hydrate Sedimentary Cores. EGU General Assembly Conference Abstracts.
Osborne, J., Yetginer, A., Halliday, T., et al., 2011. The Future of Deepwater Site Investigation: Seabed Drilling Technology. Proc. Int. Symp. Frontiers in Offshore Geotechnics II. ISFOG.
Pang, X.Q., Jia, C.Z., Wang, W.Y., 2015. Petroleum geology features and research developments of hydrocarbon accumulation in deep petroliferous basins. Petrol. Sci. 12 (1), 1–53. https://doi.org/10.1007/s12182-015-0014-0.
Pinkett, J., Westacott, D., 2016. Innovative Sidewall Pressure Coring Technology Improves Reservoir Insight in Multiple Applications. SPWLA 57th Annual Logging Symposium.
Priest, J.A., Druce, M., Roberts, J., et al., 2015. PCATS Triaxial: A new geotechnical apparatus for characterizing pressure cores from the Nankai Trough, Japan. Mar. Petrol. Geol. 66, 460–470. https://doi.org/10.1016/j.marpetgeo.2014.12.005.
Qin, H.W., Chen, Y., Gu, L.Y., et al., 2009. Research progress of fidelity sampling technology for seabed sediments. J. Tropical. Oceanograph. 28 (4), 42–48. https://doi.org/10.3969/j.issn.1009-5470.2009.04.008 (in Chinese).
Qin, H.W., Gu, L.Y., Li, S.L., et al., 2005. Pressure tight piston corer–A new approach on gas hydrate investigation. China Ocean Eng. 19 (1), 121–128. https://doi.org/10.3321/j.issn:0890-5487.2005.01.011.
Rothwell, R., Rack, F., 2006. New techniques in sediment core analysis: An introduction. Geological Society, London, Special Publications. 267, pp. 1–29. https://doi.org/10.1144/GSL.SP.2006.267.01.01.
Santamarina, J.C., Dai, S., Terzariol, M., et al., 2015. Hydro-bio-geomechanical properties of hydrate-bearing sediments from Nankai Trough. Mar. Petrol. Geol. 66. https://doi.org/10.1016/j.marpetgeo.2015.02.033.
Santamarina, J.C., Winters, W., Dai, S., et al., 2012a. Pressure core characterization tools to enhance gas hydrate field programs. Fire in the ice: Department of Energy, Office of Fossil Energy. National Energy Technology Laboratory, Methane Hydrate News Letter 12, 7–9.
Santamarina, J.C., Dai, S., Jang, J., et al., 2012b. Pressure core characterization tools for hydrate-bearing sediments. Sci. Drill. 14, 44–48. https://doi.org/10.5194/sd-14-44-2012.
Schultheiss, P., Francis, T., Holland, M., et al., 2006. Pressure coring, logging and subsampling with the HYACINTH system. Geo. Soc. London, Special Publ. 267, 151–163. https://doi.org/10.1144/GSL.SP.2006.267.01.11.
Schultheiss, P., Holland, M., Humphrey, G., 2009. Wireline coring and analysis under pressure: recent use and future developments of the HYACINTH system. Sci. Drill. 7. https://doi.org/10.5194/sd-7-44-2009.
Schultheiss, P., Holland, M., Roberts, J., et al., 2017. Advances in wireline pressure coring, core handling, and core analysis related to gas hydrate drilling investigations. Proceedings of the 9th International Conference on Gas Hydrates. ICGH 2017.
Schultheiss, P., Holland, M., Roberts, J., et al., 2011. PCATS: pressure core analysis and transfer system. Proceedings of the 7th International Conference on Gas Hydrates. ICGH 2011), Edinburgh, UK.
Skiba, S., Strukov, D., Sagidullin, A., et al., 2020. Impact of biodegradation of oil on the kinetics of gas hydrate formation and decomposition. J. Petrol. Sci. Eng. 192, 107211. https://doi.org/10.1016/j.petrol.2020.107211.
Su, Y., 2019. Environmentally-friendly sealed coring technology for unconsolidated formations 2019. Oil Drill. Prod. Technol. 41 (5), 592–596 (in Chinese).
Sun, S.Q., Zhang, Q., Zheng, K.G., et al., 2020. Technology and equipment of sealed coring for accurate determination of coalbed gas content in ground well. J. China Coal Soc. 45 (7), 2523–2530. https://doi.org/10.13225/j.cnki.jccs.DZ20.0672 (in Chinese). https://kns.cnki.net/kcms/detail/detail.aspx?dbcode=CJFD&dbname=CJFDLAST2020&filename=MTXB202007021&uniplatform=NZKPT&v=efkKbEfKyc1Ws3C-WdBeVPOcq_PUkvCziGkJ2LvwCkIRFIzmiXt3aT0hrwZ-393m.
Sun, Y., Wang, Y., Lü, X., et al., 2015. Hole-bottom freezing method for gas hydrate sampling. J. Nat. Gas Sci. Eng. 25, 271–283. https://doi.org/10.1016/j.jngse.2015.05.011.
Suzuki, K., Schultheiss, P., Nakatsuka, Y., et al., 2015. Physical properties and sedimentological features of hydrate-bearing samples recovered from the first gas hydrate production test site on Daini-Atsumi knoll around Eastern Nankai Trough. Mar. Petrol. Geol. 66. https://doi.org/10.1016/j.marpetgeo.2015.02.025.
Wakishima, R., Imazato, M., Nara, M., et al., 1998. The development of a pressure temperature core sample (PTCS) for the recovery of in-situ methane hydrates. Int Symp Methane Hydrates Proc 107–120.
Wang, J., He, J., Lv, X., et al., 2021. Numerical analysis of the gas recovery performance in hydrate reservoirs with various parameters by stepwise depressurization. J. Petrol. Sci. Eng. 203, 108670. https://doi.org/10.1016/j.petrol.2021.108670.
Wang, L., Li, Y., Wu, P., et al., 2020. Physical and mechanical properties of the overburden layer on gas hydrate-bearing sediments of the South China sea. J. Petrol. Sci. Eng. 189, 107020. https://doi.org/10.1016/j.petrol.2020.107020.
Wang, W.S., Zhang, H.C., Yan, J., 2014. Critical technology of scientific coring of hard rocks in ultra-deep wells. Explor. Eng. 41 (1), 9–12. https://doi.org/10.3969/j.issn.1672-7428.2014.01.004 (in Chinese).
Wei, G., Pengyu, Z., Xiang, Y., et al., 2020. Development and application of hole-bottom freezing drilling tool for gas-hydrate-bearing sediment sampling. Ocean Eng. 203, 107195. https://doi.org/10.1016/j.oceaneng.2020.107195.
Wu, H., 2008. Research on Deep-Sea Hydrothermal *In-Situ* Exploration Technology and its Prototype System Integration. Ph.D Dessertation. Zhejiang University.

Xie, H., Gao, F., Ju, Y., 2015. Research and development of rock mechanics in deep ground engineering. Chin. J. Rock Mech. Eng. 34, 2161–2678. https://doi.org/10.13722/j.cnki.jrme.2015.1369 (in Chinese).
Xie, H.P., Liu, T., Chen, L., et al., 2018a. Deep Rock Quality-Guaranteeing Coring Device. China. CN209261521U. 2018-12-06.
Xie, H.P., Liu, T., Chen, L., et al., 2018b. Deep Rock Quality-Preserving and Coring Device and Coring Method Thereof. China. CN109403900A. 2018-12-06.
Xie, H., Konietzky, H., Zhou, H.W., 2019. Special issue "deep mining.". Rock Mech. Rock Eng. 52 (5), 1415–1416. https://doi.org/10.1007/s00603-019-01805-9.
Xie, H.P., Gao, M.Z., Zhang, R., et al., 2020a. Deep Rock In-Situ Quality-Guaranteeing Coring Device and While-Drilling Film-Forming Coring Method Thereof. China. CN111734332A. 2020-07-29.
Xie, H.P., Gao, M.Z., Zhang, R., et al., 2020b. Study on concept and progress of in situ fidelity coring of deep rocks. Chin. J. Rock Mech. Eng. 39 (5), 865–876. https://doi.org/10.13722/j.cnki.jrme.2020.0138 (in Chinese).
Xie, H.P., Gao, M.Z., Zhang, R., et al., 2020c. While Drilling Film Formation Simulation Device and while Drilling Film Formation Coring Method. China. CN212689971U. 2020-07-29.
Yang, L., Su, Y., Luo, J., et al., 2020. Development of the GW-CP194-80A pressure-retaining corer. Nat. Gas. Ind. 40 (04), 91–96 (in Chinese). https://kns.cnki.net/kcms/detail/detail.aspx?dbcode=CJFD&dbname=CJFDLAST2020&filename=TRQG202004017&uniplatform=NZKPT&v=aQy0Dkmfw3yh1V4S7vY1mWoFDoyaVn_n3HjPlnihXDH94zHY7tlvG2KZ6LXsk61U.
Yang, S.M., Tao, W.Q., 2006. Heat Transfer, fourth ed. Higher Education Press, Beijing.
Yang, X.G., Guo, S.B., 2020. Porosity model and pore evolution of transitional shales: an example from the Southern North China Basin. Petrol. Sci. 17 (6), 1512–1526. https://doi.org/10.1007/s12182-020-00481-7.
Yetginer, G., Tjelta, T., 2010. Seabed Drilling vs Surface Drilling - A Comparison. Int. Symp. Frontiers in Offshore Geotechnics. ISFOG.
Yoneda, J., Masui, A., Konno, Y., et al., 2015a. Mechanical behavior of hydrate-bearing pressure-core sediments visualized under triaxial compression. Mar. Petrol. Geol. 451–459. https://doi.org/10.1016/j.marpetgeo.2015.02.028.
Yoneda, J., Masui, A., Konno, Y., et al., 2015b. Mechanical properties of hydrate-bearing turbidite reservoir in the first gas production test site of the Eastern Nankai Trough. Mar. Petrol. Geol. 471–486. https://doi.org/10.1016/j.marpetgeo.2015.02.029.
Yun, T.S., Narsilio, G., Santamarina, J., et al., 2006. Instrumented pressure testing chamber for characterizing sediment cores recovered at in situ hydrostatic pressure. Mar. Geol. 229, 285–293. https://doi.org/10.1016/j.margeo.2006.03.012.
Yun, T.S., 2005. Mechanical and Thermal Study of Hydrate Bearing Sediments. Ph.D Dessertation. Georgia Institute of Technology.
Zhang, D.Y., Jiang, Z.L., Yu, P., et al., 2006. Deepwater and Shallow Holes Heat Preservation and Pressure Retaining Coring Tools for Gas Hydrate. China. CN1818323. 2006-03-20.
Zhang, L., Chu, J., Li, N., 2019a. Application and Implementation of Steinmetz Solid. Journal of Physics: Conference Series. IOP Publishing.
Zhang, X.S., Wang, H.J., Ma, F., et al., 2016. Classification and characteristics of tight oil plays. Petrol. Sci. 13 (1), 18–33. https://doi.org/10.1007/s12182-015-0075-0.
Zhang, Z., Xie, H., Zhang, R., et al., 2019b. Deformation damage and energy evolution characteristics of coal at different depths. Rock Mech. Rock Eng. 52 (5), 1491–1503. https://doi.org/10.1007/s00603-018-1555-5.
Zhao, Z.Y., Xie, H.P., Liu, T., et al., 2020. In situ curing of a polymer film for light-proof coring of deep rocks with preservation of rock quality and moisture. Adv. Civ. Eng. 8843779. https://doi.org/10.1155/2020/8843779, 2020.
Zhou, H.W., Xie, H.P., Zuo, J.P., et al., 2010. Experimental study of the effect of depth on mechanical parameters of rock. Chin. Sci. Bull. 55 (34), 3276–3284. https://doi.org/10.1360/972010-786 (in Chinese).
Zhu, H., Liu, Q., Deng, J., et al., 2013. A pressure and temperature preservation system for gas-hydrate-bearing sediments sampler. Petrol. Sci. Technol. 31, 652–662. https://doi.org/10.1080/10916466.2010.531352.
Zuo, J.P., Chai, N.B., Zhou, H.W., 2011. Study on the effect of buried depth on failure and energy characteristics of the basalt. Chin. J. Undergr. Space Eng. 7 (6), 1174–1180. https://doi.org/10.3969/j.issn.1673-0836.2011.06.023 (in Chinese).